Acta Geologica Polonica, Vol. 73 (2023), No. 4, pp. 741–772
DOI: 10.24425/agp.2023.145629

Tracing the latest Jurassic–earliest Cretaceous paleoenvironment evolution in swell carbonate facies: a case study of the High-Tatric succession (Central Western Carpathians, Tatra Mts, Poland)

DAMIAN GERARD LODOWSKI[1, 2] and JACEK GRABOWSKI[2]

[1] *University of Warsaw, Faculty of Geology, Żwirki i Wigury 93, 02-089 Warszawa, Poland; e-mail: damian.lodowski@uw.edu.pl*
[2] *Polish Geological Institute-National Research Institute, Rakowiecka 4, 00-975 Warszawa, Poland; e-mails: damian.lodowski@pgi.gov.pl; jacek.grabowski@pgi.gov.pl*

ABSTRACT:

Lodowski, D.G. and Grabowski, J. 2023. Tracing the latest Jurassic–earliest Cretaceous paleoenvironment evolution in swell carbonate facies: a case study of the High-Tatric succession (Central Western Carpathians, Tatra Mts, Poland). *Acta Geologica Polonica*, **73** (4), 741–772. Warszawa.

This paper presents an interpretation of sedimentologic, paleomagnetic, and geochemical data collected in the Upper Kimmeridgian–Valanginian carbonates of the Giewont series (Giewont and Mały Giewont sections, High-Tatric succession, Western Tatra Mountains, Poland). The studied succession provides insight into the sedimentary conditions prevailing in the South Tatric Ridge (Tatricum), a submarine elevation located between the Zliechov Basin (Fatricum) and the Vahic (=South Penninic) Ocean. The sedimentary sequence includes micrites, pseudonodular limestones, cyanoid packstones, lithoclastic packstone, and encrinites. The results are discussed with regards to their significance for detrital input, paleoclimate, and paleoproductivity, which in turn are considered in the context of both local and regional paleoenvironmental trends and events. The greatest depositional depths during the latest Kimmeridgian–earliest Tithonian are documented by the occurrence of pseudonodular limestones. A Tithonian shallowing trend is demonstrated via the increasing size and roundness of cyanoids, while the final (?)emergence and erosion in the South Tatric Ridge is documented by earliest Cretaceous disconformities. This process might have been related to both falling sea-level during the major eustatic regressive cycle and tectonic uplift caused by the mutually related (re)activation in the Neotethyan Collision Belt and rifting in the Ligurian-Penninic-Vahic Oceans. The highest lithogenic influx (although still low; max 0.5% of Al content) during the Late Kimmeridgian is considered as associated with relatively humid climate conditions, whereas a subsequent decreasing trend is thought to result from aridification during the latest Kimmeridgian–earliest Tithonian. Ultimately, deposition in the High-Tatric zone was affected by both large-scale environmental perturbations characteristic of the latest Jurassic (climate changes, variations in sea-water pH, monsoonal upwelling, lithogenic input, etc.), as well as local sedimentary controls, predominantly the oxygenation state of bottom waters and tectonic movements.

Key words: Microfacies; Geochemistry; Rock magnetism; Lithogenic input; Paleoclimate; Monsoonal upwelling; Hypoxia; Paleoproductivity; Central Western Carpathians.

INTRODUCTION

The latest Jurassic–earliest Cretaceous interval constitutes a period with considerable paleoenvironmental perturbations, which manifest in both facies development (for instance, in the switch from radiolarite- to carbonate-dominated deposition or subsequent drastic limitation of the *Ammonitico Rosso*

facies; e.g., Cecca *et al*. 1992; Jach and Reháková 2019) and paleoecologic processes (for instance, several nannofossil calcification events, radiolarian to calpionellid-dominated depositional turnover, and the waning of *Saccocoma*-dominated carbonates; Casellato 2009; Grabowski *et al*. 2019; Jach and Rehákova 2019; Casellato and Erba 2021; Lodowski *et al.* 2022a). These disturbances likely resulted from the interplay of numerous factors, such as biotic productivity, water column pH and redox state (e.g., Weissert and Mohr 1996, Weissert and Erba 2004, Weissert *et al*. 1998) climatic changes (Abbink *et al*. 2001, Hesselbo *et al*. 2009, Föllmi 2012, Bover-Arnal and Strasser 2013), eustasy (Hardenbol *et al.* 1998; Haq 2014, 2018), oceanographic phenomena (e.g., De Wever *et al*. 2014) and/or tectonics (e.g., Stampfli and Hochard 2009; Missoni and Gawlick 2011; Plašienka 2018). When attempting to prepare consistent paleoenvironment interpretations and models it is crucial to determine whether, and to what extent, these mechanisms manifest in different tectonic units.

In this context, insight into both typical pelagic and considerably shallower sedimentary zones is provided by the sections in the Tatra Mts (Central Western Carpathians, e.g., Jach *et al.* 2014; Pszczółkowski *et al*. 2016, Pszczółkowski 2018). During the Late Jurassic–Early Cretaceous, the Central Western Carpathians were located between the Alpine Atlantic (Ligurian-Penninic-Vahic Oceans) to the north and the Neo-Tethys Ocean to the south (Text-fig. 1D and E). Although intermittent, the record of the Jurassic/Cretaceous transition in relatively shallow facies can be traced on the northern slopes of Mt. Giewont (High-Tatric succession, Poland; Lodowski *et al.* 2022b). This study attempts to reconstruct the late Kimmeridgian to Valanginian history of the High-Tatric Giewont series based on detailed microfacies analysis and high-resolution geochemical and rock-magnetic data basing on the stratigraphic research of Lodowski *et al.* (2022b). The results are discussed in the context of both local and regional paleoenvironmental trends and events, providing new data on correlation between the Western Tethyan and Subboreal domains, with special focus on the paleoclimate evolution.

GEOLOGICAL SETTING AND PREVIOUS STUDIES

The Tatra Mountains are located in the northernmost Central Western Carpathians (CWC), part of the vast Alpine-Carpathian-Dinaric orogen (Text-fig. 1). The Tatras are composed of a crystalline core and a latest Paleozoic–Mesozoic sedimentary cover. The crystalline basement consists of the granitoids of the High Tatra Mts, as well as granitoid and metamorphic rocks of the Western Tatra Mts, whereas the sedimentary cover consists of: 1) High-Tatric autochthonous cover and nappes; and 2) Sub-Tatric nappes (see Jurewicz, 2005 and references therein for further details). The High-Tatric succession records the deposition on the (South) Tatric Ridge, facing the Vahic Ocean to the north and the Zliechov Basin to the south (e.g., Häusler *et al.* 1993; Plašienka 2018 and references therein; Text-fig. 1E).

The study area is located within the Giewont Unit, one of the High-Tatric allochthonous units, providing a record of its Early Triassic–Late Cretaceous evolution (e.g., Kotański 1959, 1961; Lefeld 1968; Lefeld *et al.* 1985). The upper Jurassic consists of the Raptawicka Turnia Limestone Formation (RTL Fm). The RTL Fm may be subdivided into three informal members: 1) pinkish pelitic limestones, with ammonites, of the lower member (Callovian–Oxfordian; Lefeld *et al*. 1985); 2) light gray *Saccocoma*-cyanoid limestones of the middle member (Oxfordian–Lower Tithonian; Lefeld *et al*. 1985; Lodowski *et al*. 2022b); and 3) nearly black cyanoid limestones of the upper member (Tithonian; Lodowski *et al.* 2022b; "black Valanginian limestones" of Lefeld *et al*. 1985). According to Lodowski *et al*. (2022b), the top of the RTL Fm in the Giewont section is erosively cut by a latest Tithonian–Early (?Late) Berriasian disconformity. The succession continues with, limited in thickness, Upper Berriasian–Lower Valanginian lithoclastic limestone, which is followed by another (approximately late Early–early Late Valanginian) lacuna and Late Valanginian (?and Hautervian) encrinites (both Wysoka Turnia Limestone Formation, WTL Fm; Lefeld 1968; Lodowski *et al*. 2022b). Interestingly, in the vicinity of the Osobita massif (westernmost Tatra Mts; Text-fig. 1B), the Upper Valanginian of the WTL Fm is separated from the Tithonian RTL Fm by an eruptive series of limburgites and tuffites, estimated as Tithonian–Berriasian in age (Kotański and Radwański 1959; Staniszewska and Ciborowski 2000; Madzin *et al*. 2014; Lodowski *et al*. 2022b). Madzin *et al*. (2014) provided also an evidence for a latest Tithonian–?Early Valanginian age of the volcanism, with an emplacement climax during the Late Berriasian–?Early Valanginian.

Section descriptions

This research considers data obtained during fieldwork conducted in two closely-spaced locali-

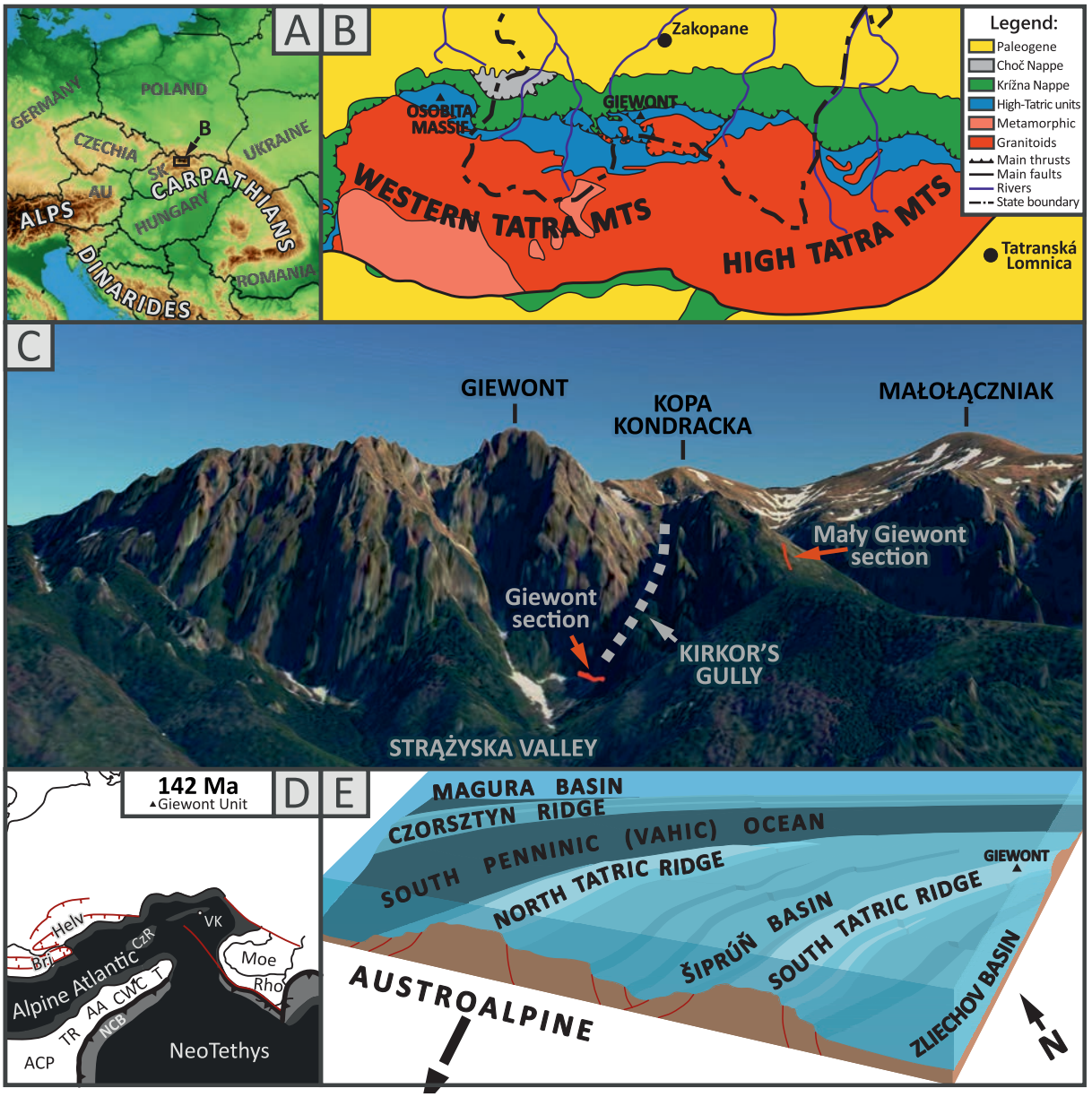

Text-fig. 1. Geological setting of the study area. (A) Location of the Tatra Mountains in Europe; Abbreviations: AU – Austria; SK – Slovakia. (B) Geological map of the Tatra Mts (modified after Nemčok *et al.* 1994 and Jurewicz 2005). (C) Localities of the studied sections. (D) Simplified paleogeographic map of the circum Carpathian region during the Berriasian; modified after Stampfli and Hochard (2009) and Grabowski *et al.* (2019). Abbreviations: AA – Austro Alpine; ACP – Adriatic Carbonate Platform; CWC – Central Western Carpathians; NCB – Neotethyan Collision Belt; Bri – Brianconnais; CzR – Czorsztyn Ridge (Pieniny Klippen Belt); Helv. – Helvetic units; Moe – Moesian Platform; Rho – Rhodopes; T – Tisia; TR – Transdanubian Range; VK – Velykyi Kamianets (Pieniny Klippen Belt). (E) Conceptual paleogeographic reconstruction of the Tatricum and adjacent area during the latest Jurassic; with respect to Plašienka (1995).

ties: the Mały Giewont (49°15'09" N; 19°55'30" E) and the Giewont (49°15'15" N; 19°55'52" E) sections (Text-figs 1–2). These were previously described by Pszczółkowski *et al.* (2016) and Lodowski *et al.* (2022b), and correlated by Lodowski *et al.* (2022b); therefore, only the most characteristic stratigraphic and microfacies features of the Jurassic/Cretaceous transition in the Giewont series are outlined below.

The studied part of the Giewont series provides a record of c. 80 m thick upper Kimmeridgian–upper Valanginian strata, covering the transition from the RTL Fm to the WTL Fm (Text-fig. 2). The stra-

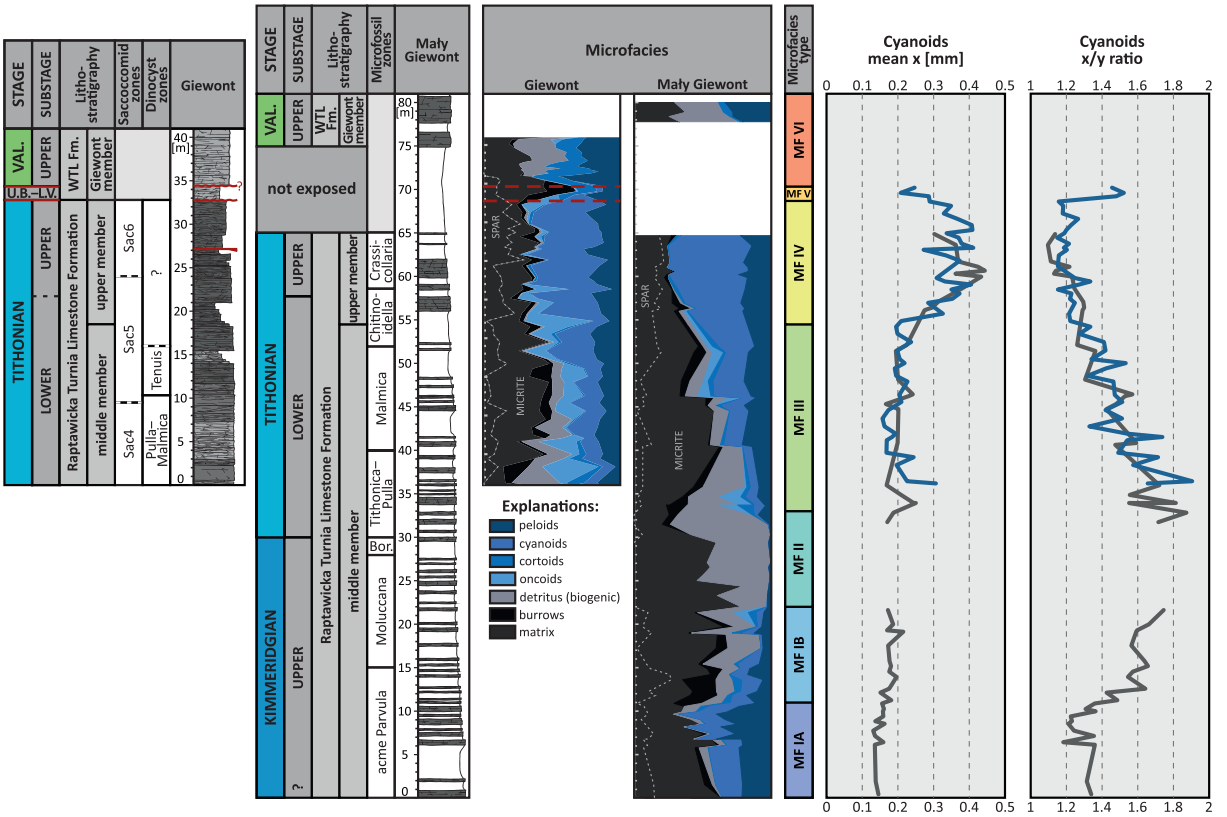

Text-fig. 2. Microfacies and cyanoid morphometry of the Giewont and Mały Giewont sections. Microfacies succession and correlation between sections after Lodowski *et al.* (2022b). Gaps in morphometric logs correspond to intervals barren in cyanoids. Mean x is adopted as a size proxy, whilst x/y ratio as a sphericity indicator; see text for further discussion. Blue – Giewont section; gray – Mały Giewont section. Abbreviations: U.B.–L.V. – Upper Berriasian–Lower Valanginian; VAL. – Valanginian; WTL Fm – Wysoka Turnia Limestone Formation; Bor. – Borzai.

tigraphy of the interval is based on calcareous dinocysts and calpionellids (Pszczółkowski *et al.* 2016, Lodowski *et al.* 2022b; following the scheme of Reháková 2000), and Kimmeridgian ammonites (Pszczółkowski *et al.* 2016). The lowermost part of the succession is characterized by cyanoid- (e.g., Riding 1983; see also Pszczółkowski 2018) and peloid-bearing wackestones (microfacies IA; MF IA; Text-fig. 3A) and packstones (MF IB; Text-fig. 3B) of the middle member of the RTL Fm (acme *Parvula–Moluccana* dinocyst Zones). The Kimmeridgian/Tithonian boundary interval (upper *Moluccana* to lower *Tithonica–Pulla* dinocyst Zones) is marked by pseudonodular limestones (patches of wackestones and *Saccocoma*-dominated packstones; MF II; Text-fig. 3C). Above, the rocks gradually pass into wackestones and packstones of the lower Tithonian (MF III; upper part of the *Tithonica–Pulla* dinocyst Zone to the lower part of the *Chitinoidella* calpionellid Zone; Text-fig. 3D–E). Within the *Chitinoidella* Zone, the record becomes dominated by cyanoids (cyanoid packstone; MF IV; Text-fig. 3F), which characterize the upper member of the RTL Fm (uppermost Lower–Upper Tithonian). The cyanoid packstones are cut by the latest Tithonian–Early (?Late) Berriasian disconformity, and followed by Upper Berriasian–Lower Valanginian lithoclastic packstones (MF V; lower beds of the Giewont Member of the WTL Fm; Text-fig. 3G). Another, presumably late Early–early Late Valanginian disconformity occurs above; the succession continues in the Upper Valanginian encrinites of the upper beds of the Giewont Member (crinoidal packstones; MF VI; Text-fig. 3H), which can be compared to the Valanginian Spisz Limestone Fm of the

Text-fig. 3. Microfacies of the Upper Kimmeridgian–Upper Valanginian of the Giewont series. MG – Mały Giewont samples; G – Giewont samples; A – MF IA, sample MG60; B – MF IB, sample MG78 ; C – MF II, sample MG84; D – MF III, sample MG101; E – MF III, sample G16; F – MF IV, sample G28.9; G – MF V, sample G29.4; H – MG VI, sample G38. Abbreviations: A – ammonite; C – cyanoid; Co – cortoid; Cr – crinoid; GA – *Globochaete alpina*; L – lithoclast; O – ostracod; P – peloid; R – radiolarian; S – *Saccocoma* skeletal element. →

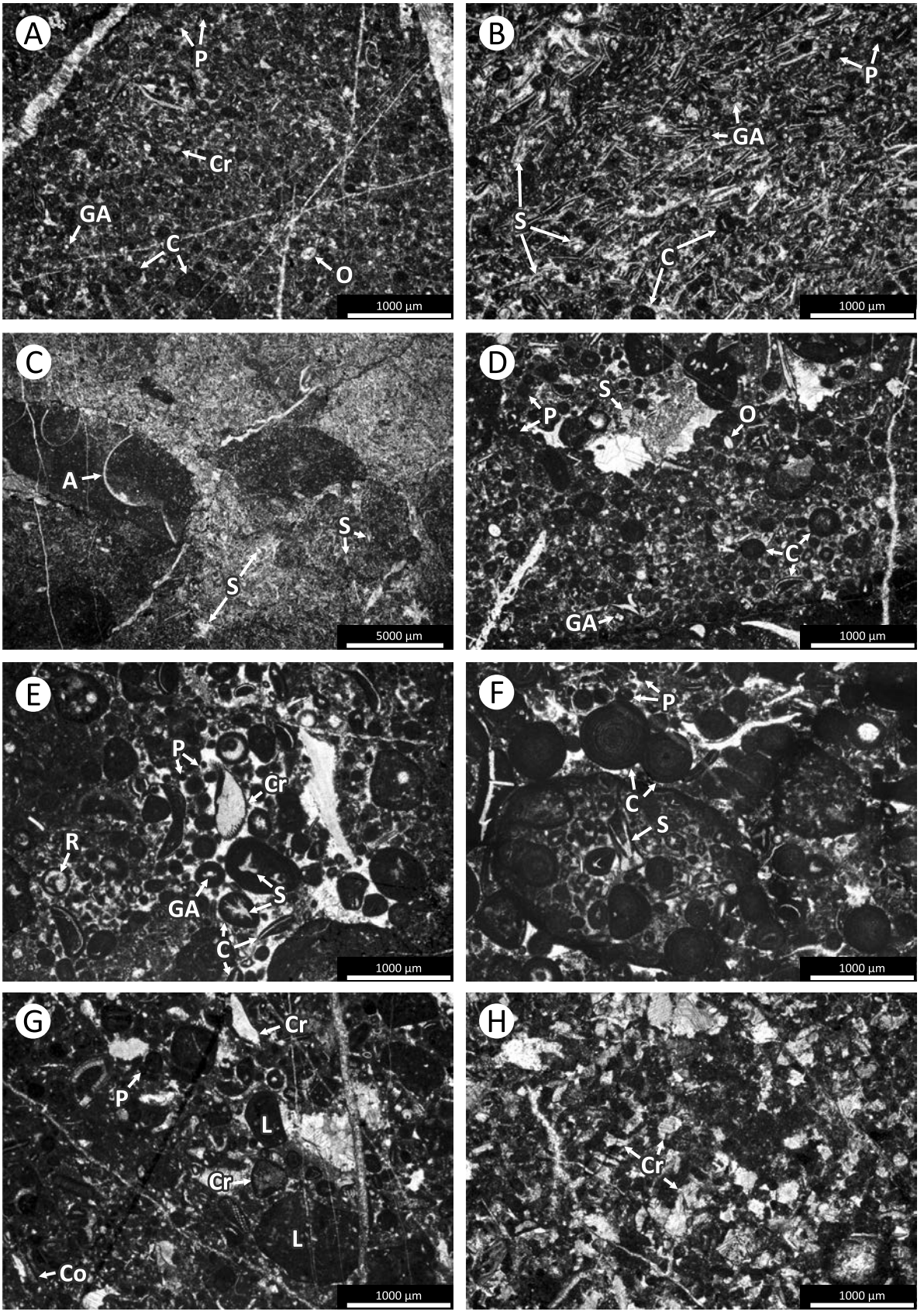
A
P
Cr
GA
C
O
1000 µm
B
P
GA
S
C
1000 µm
C
A
S
S
5000 µm
D
S
P
O
C
GA
1000 µm
E
P
Cr
R
GA
S
C
1000 µm
F
P
C
S
1000 µm
G
Cr
P
L
Cr
L
Co
1000 µm
H
Cr
1000 µm

Pieniny Klippen Belt (Birkenmajer 1977) (see also Text-fig. 2; Lodowski *et al.* 2022b).

MATERIALS AND METHODS

All the data generated and processed during the current study are available from the corresponding author upon request as Supplementary Online Material 1 (SOM 1).

Cyanoid morphometry

A total of 79 thin sections from the Giewont section, and 66 from the Mały Giewont section – the same ones as used in the microfacies analysis of Lodowski *et al.* (2022b) – were subjected to cyanoid morphometric analysis. Basic observations were performed using a Nikon ECLIPSE LV100POL microscope (Optical Microscopy Lab of the Faculty of Geology, University of Warsaw); images were taken in natural light using Nikon NIS software. The largest and smallest axis of each cyanoid was measured (x-axis: largest; y-axis: smallest); a total number of 3915 measurements were performed, of which 2010 came from the Giewont and 1905 from the Mały Giewont section. These measurements were later used for calculations of mean cyanoid size (= mean value of the x-axis) and roundness (= x-axis / y-axis).

Sedimentation rates estimations

Although depositional rates in the Giewont series cannot be precisely calculated, due to the lack of magnetostratigraphic control and/or the limited resolution of biostratigraphic data, an attempt to estimate minimum sedimentation rates of the following intervals is possible: 1) Upper Kimmeridgian (MF IA–IB); 2) the Kimmeridgian/Tithonian transition (MF II); 3) Lower Tithonian (MF III); and 4) the uppermost Lower–Upper Tithonian (MF IV). The idea is based on the fact, that in the Tithonian–Berriasian calpionellids and calcareous dinocysts are calibrated with the magnetostratigraphy (Grabowski *et al.* 2019; Casellato and Erba 2021), which enables estimations of biozonal time durations. Numeric ages are adopted from Ogg (2020), whereas stratigraphic correlation is from Lodowski *et al.* (2022b).

Magnetic susceptibility and rock magnetism

Field magnetic susceptibility (MS) measurements and some of rock magnetic investigations (isothermal remanent magnetization, IRM; anhysteretic remanent magnetization, ARM) discussed further in this study were performed by Lodowski *et al.* (2022b); herein they are interpreted in terms of their paleoenvironmental significance. Consequently, there are presented here only the methods applied in previously unpublished investigations.

Multi-frequency measurements of MS are considered herein with regards to the presence of superparamagnetic (SP; ultra-fine grained) magnetite and/or maghemite. This method relies on the fact that, with increasing frequency of an applied magnetic field, SP grains depict lower MS (Dearing *et al.* 1996). Consequently, a relative loss of frequency dependent MS (χ_{FD}) calculated from subtraction of high-frequency MS ($\chi_{15\,616\,Hz}$) from low-frequency MS ($\chi_{976\,Hz}$) is indicative of the occurrence of SP grains. Mass-normalized MS measurements were performed using an Agico MFK1-FB kappabridge (Polish Geological Institute-National Research Institute, PGI-NRI).

To identify magnetic minerals, cylindrical samples were subjected to stepwise acquisition of the IRM (in a maximum field of 1.4 T in the z-axis) and subsequent thermal demagnetization of the three-axis IRM acquired in 1.4 T (z-axis), 0.4 T (y-axis), and 0.1 T (x-axis) fields (see Lowrie 1990). These experiments were performed at the Geophysical Laboratory of the European Center of Geological Education (ECEG) in Chęciny, Poland (University of Warsaw) using a Magnetic Measurements MMPM 10 pulse magnetizer, a Magnetic Measurements TD80 oven, and an Agico JR6A spinner magnetometer. Three samples were subjected to temperature-dependent MS measurements (Magnetic Measurements TD1 oven, Agico KLY2 kappabridge; PGI-NRI) to address the potential presence of pyrite (e.g., Li and Zhang 2005).

Frequency-dependent MS measurements were controlled using Agico Safyr7 software, whereas IRM measurements were processed using Agico Rema6 software.

Gamma-ray spectrometry (GRS) and elemental geochemistry

This study considers the paleoenvironmental significance of the field GRS and laboratory ICP-MS (MA250 method, Bureau Veritas Minerals Schedule of Service & Fees 2020) measurements which were partly published and utilized for stratigraphic purposes by Lodowski *et al.* (2022b). These are supplemented with the results of measurements of numerous other elements of paleoenvironmental importance, as well as 7 new samples from the Valanginian interval.

Amongst various geochemical proxies indicative of different sedimentary and weathering processes here the following are examined: Ca/Al (to reflect relative clasticity), Zr/Al (grain size proxy; e.g., Schnetger *et al*. 2000); Zr/Rb (to reflect general changes in siliciclastic grain size; e.g., Bassetti *et al*. 2016) as well as Chemical Index of Alteration (CIA; Nesbitt and Young 1982), Ti/K and Al/K (both related to humidity of paleoclimate, e.g., Wei *et al*. 2003, 2006; Tian *et al*. 2011). CIA, which is indicative of intensity of climate-related removal of mobile elements, was calculated with respect to the following formula:

$$CIA = [\frac{Al_2O_3}{Al_2O_3 + CaO^* + Na_2O + K_2O}] \times 100\%$$

where CaO* is the amount of CaO incorporated in the silicate fraction of the rock. To do that, elemental concentrations of given elements were stoichiometrically converted to their oxide equivalents, whereas silicate CaO is approximated to the proportion of Na_2O (i.e., McLennan 2001). Due to moderate correlation between Na and Al (PCC = 0.75), the detrital fraction of Na was approximated by a subtraction of Na_{EXCESS} (see below) from Na_{SAMPLE}. However, it must be noted, that even in the same stratigraphic horizons, the content of Na systematically differs between the Giewont and Mały Giewont c. 3 times (see SOM 1). Consequently, the Kimmeridgian CIA, which is ensured only by the data from the Mały Giewont section, should be regarded as not very reliable.

To investigate whether the sediments were subjected to oxygen depletion, both GRS and laboratory uranium concentrations have been recalculated with respect to the authigenic U formula of Jones and Manning (1994):

$$\text{Authigenic U} = U_{SAMPLE} - (\frac{Th_{SAMPLE}}{3})$$

Additionally, the U/Th (e.g., Jones and Manning 1994) and Fe/Al (Algeo and Liu 2020) ratios were calculated. To evaluate the paleoredox signal recorded in Mo and V (e.g., Algeo and Li 2020; Algeo and Liu 2020) their enrichment factors (EF) were calculated, following the formula of Li and Schoonmaker (2003):

$$EF_X = \frac{X_{SAMPLE}/Al_{SAMPLE}}{X_{AVERAGE\ SHALE}/Al_{AVERAGE\ SHALE}}$$

where X is the element considered.

Phosphorus, Ba, and Zn are well known from their nutrient-type distribution and, in the case of P and Zn, from their importance for living organisms (e.g., Tribovillard *et al.* 2006; Robbins *et al.* 2016). In marine environments, they are readily bound by plankton and/or adsorbed by organic particles, and subsequently released within the water column or sediment (i.e., remineralized) via taphonomic processes. As a result, variations in their abundance (or accumulation rates) may be interpreted either in terms of paleoproductivity and its controls, or disruption in their uptake processes (recycling in the water column, cf. Falkowski 2012). To exclude detrital contributions, their biological ('excess') concentrations have been calculated following the equation: $X_{EXCESS} = X_{SAMPLE} - (Al_{SAMPLE} \times D)$, where X is the examined element while D is a "detrital" constant, approximated as the lowest non-protruding X/Al ratio in the entire dataset (Rutsch *et al*. 1995; Shen *et al*. 2015; Grabowski *et al*. 2021b). This enables an estimation of sea-surface fertilization while taking into account the local characteristics of lithogenic influx.

RESULTS

Sedimentologic observations

Cyanoid morphometry

Upper Kimmeridgian cyanoids are characterized by small sizes and decreasing roundness, until they ultimately disappear within the uppermost Kimmeridgian *Moluccana* dinocyst Zone (Text-fig. 2). Cyanoids reappear in the lowermost Tithonian (*Tithonica–Pulla* dinocyst Zone, slightly below the base of the Giewont section), from where a trend of increasing sphericity continues to the topmost Tithonian. In parallel, their mean size also increases; however, this phenomenon becomes clear only above the base of the upper member of the RTL Fm (uppermost Lower Tithonian *Chitinoidella* calpionellid Zone). Cyanoids reach their maximum size (with mean slightly exceeding 0.4 mm), and roundness (mean x/y ratio below 1.2) within the Upper Tithonian *Crassicollaria* calpionellid Zone. Above, in the Upper Berriasian–Lower Valanginian lithoclastic packstone (MF V), they are rare, relatively small and elongated, and are totally absent within the Late Valanginian encrinites (MF VI).

Sedimentation rates

On the basis of ammonite findings, Lodowski *et al*. (2022b; see also Pszczółkowski *et al.* 2016) ascertained that the base of the investigated Giewont series falls very near to the Lower/Upper Kimmeridgian

boundary; therefore, it is approximated here to the base of magnetozone M24Ar (152.3 Ma). The pseudonodular limestone facies (MF II) appears in the middle part of the *Moluccana* dinocyst Zone, which enables a rough correlation with the base of magnetozone M23n (149.8 Ma; see also Grabowski *et al.* 2019). When further comparison is made to the Velykyi Kamianets section of the Pieniny Klippen Belt (Grabowski *et al.* 2019; see also fig. 13 in Lodowski *et al.* 2022b), the top of MF II may be correlated with the end of the decreasing $\delta^{13}C$ trend, hence near the M22n/M22r boundary (148.5 Ma). In turn, the following MF III interval continues up to the middle part of the *Chitinoidella* calpionellid Zone, slightly below the Lower/Upper Tithonian boundary. Based on the usual range of the *Chitinoidella* Zone (e.g., Casellato and Erba 2021), the top of MF III is approximated here to the base of magnetozone M20r (145.7 Ma). Finally, as the MF IV interval does not reach the Tithonian/Berriasian boundary, its top is arbitrary designated to fall within magnetozone M19n (143.5 Ma).

Consequently, the approximated sedimentation rates for the MF IA–IB interval are, at a minimum, 10 m/Ma. In the case of the MF II interval, these were c. 8.5 m/Ma, whereas for the MF III and MF IV intervals they were c. 7.5 and 6.5 m/Ma, respectively. Such results point to a secular decline of the depositional rate during the Late Kimmeridgian–Tithonian.

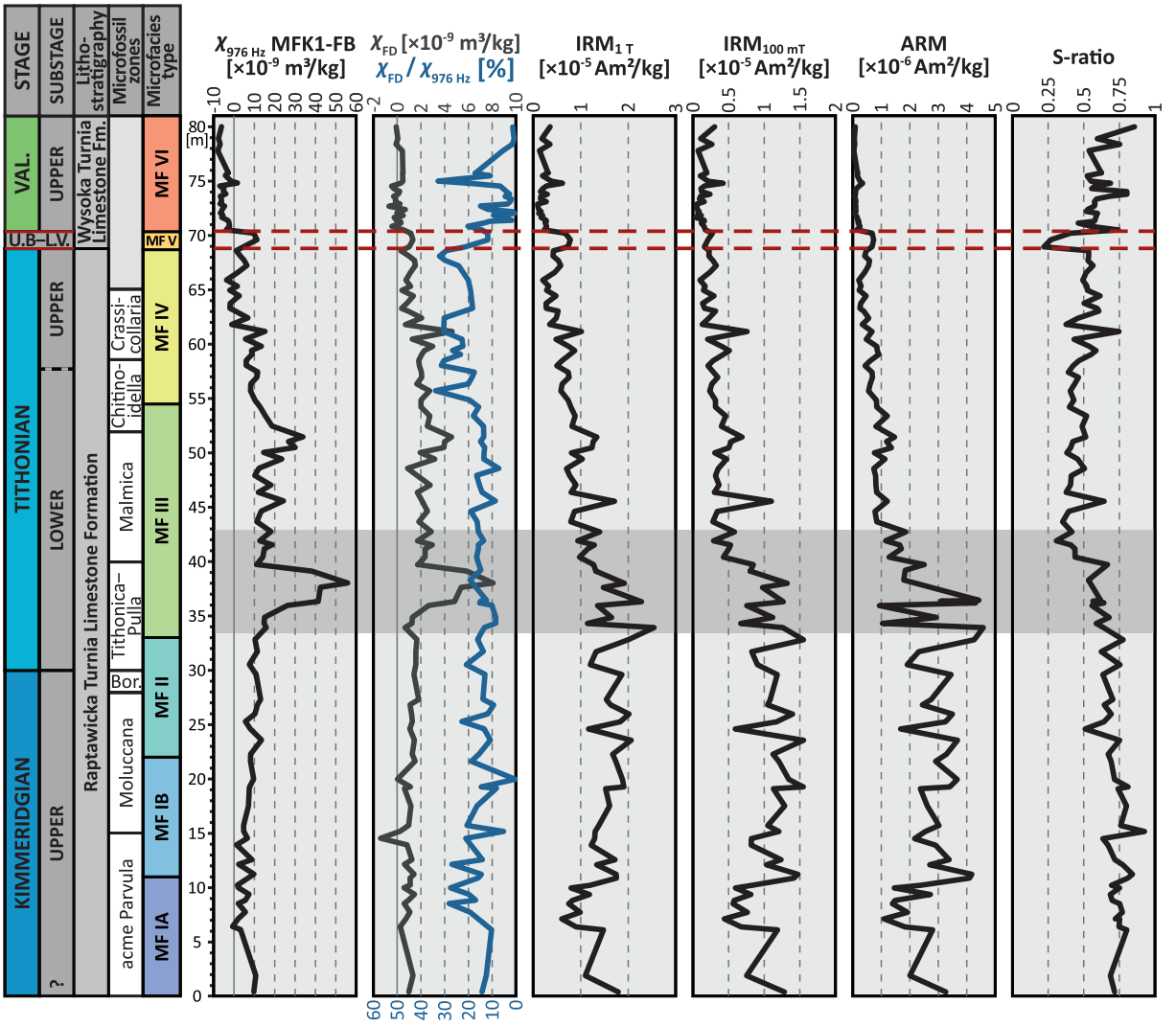

Text-fig. 4. Composite low-frequency (976 Hz) MS, frequency dependent MS (χFD), IRM_{1T}, IRM_{100mT}, ARM and S-ratio logs from the Giewont series of the High-Tatric succession. IRM_{100mT} is presented in absolute values (modulus). Note inverse scale for χ_{FD} / $\chi_{976\ Hz}$ log. Gray belt indicates an interval of rock magnetic perturbations. Abbreviations: VAL. – Valanginian; U.B.–L.V. – Upper Berriasian–Lower Valanginian; Bor. – Borzai. IRM, ARM and S-ratio logs come from Lodowski *et al.* (2022b).

Rock magnetism

Magnetic susceptibility

The MS log of the Giewont series (Text-fig. 4) may be divided in five intervals with clearly distinct characteristics: 1) the Upper Kimmeridgian (MFI–II), characterized by slightly increasing MS (0–15 × 10^{-9} m^3/kg); 2) the Lower Tithonian, with elevated MS values (MF III; up to 60 × 10^{-9} m^3/kg, with mean c. 20 × 10^{-9} m^3/kg); 3) the uppermost Lower–Upper Tithonian (MF IV), with generally decreasing MS (15–0 × 10^{-9} m^3/kg); 4) the Upper Berriasian–Lower Valanginian (MF V), with slightly elevated MS (c. 10 × 10^{-9} m^3/kg); and 5) the Upper Valanginian (MF VI), presenting near-zero (negative) MS.

Almost identical variations are observed within the frequency-dependent MS log (Text-fig. 4). χ_{FD} manifests positive values through most of the succession (besides the MF VI interval, where $\chi_{976\ Hz}$ tends towards, and below, zero); the relative MS loss ($|\chi_{FD} / \chi_{976\ Hz}|$%) usually ranges between 15–20%, and is higher only in the MF IA / MF IB transition interval and within the upper part of MF IV. When χ_{FD} is plotted against $\chi_{976\ Hz}$, it may be observed that all datapoints cluster along a single trend line, regardless of the stratigraphic interval (Text-fig. 5A). In contrast, a crossplot of χ_{FD} and IRM_{1T} distinguishes two populations: 1) samples from the MF I–II and VI intervals, with relatively stable χ_{FD} and variable IRM_{1T}; and 2) those from the MF III–V interval, characterized by more, or less, proportional variations in both parameters (Text-fig. 5B).

Thermal demagnetization of three-axis IRM and MS variations during thermal treatment

Low coercivity fraction (0.1 T) characterized by high and relatively narrow-ranged unblocking temperatures (550–575°C) is indicative of coarse-grained magnetite (e.g., A, D, G on Text-fig. 6). In turn, medium coercivity (0.4 T) particles which demagnetize within a wide range of moderate temperatures (200–450°C; e.g., B, F, I on Text-fig. 6) are suggestive of various minerals from a magnetite group, presumably fine-grained magnetite, yet also maghemite and/or titanomagnetites cannot be excluded. The occurrence of fine-grained magnetite particles can be unequivocally stated when 0.4 T fraction demagnetizes at, or near, 575°C (e.g., B, D, K on Text-fig. 6). Within the hard magnetic fraction (1.4 T), three characteristic ranges of unblocking temperatures were observed: 80–120°C, 300–350°C and above 670°C. These might be interpreted as a manifestation of goethite (e.g., Text-fig. 6A, K), pyrrhotite (or pigmentary hematite; e.g., Text-fig. 6D, L) and hematite (e.g., Text-fig. 6C, K), respectively.

The MS variations during thermal treatment (Text-fig. 7) depict decreasing susceptibilities up to 450°C, suggestive of inversion from maghemite to hematite (e.g., Liu *et al.* 2005). Above 450°C, a significant increase in MS is observed in each examined sample, which points to the presence of pyrite (e.g., Li and Zhang 2005). It is noteworthy that the MS have higher initial values and increases considerably more in sample MG99 (40.8 m) than in (the stratigraphically lower) samples MG96 (36 m) and MG71 (12.1 m).

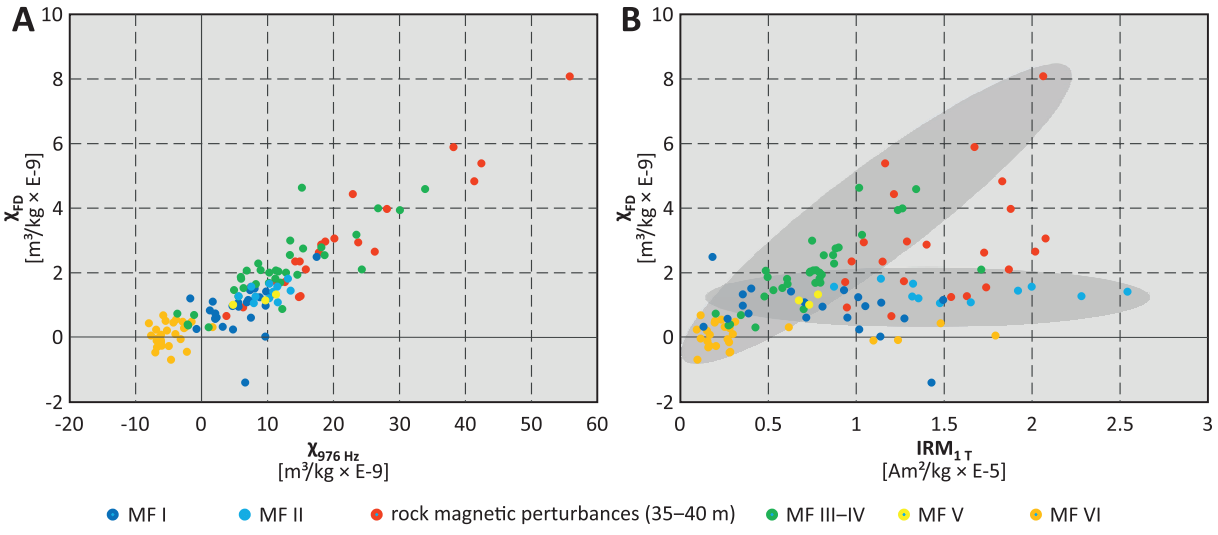

Text-fig. 5. Crossplots of A) frequency dependent MS (χFD) versus low-frequency field MS (χ976 Hz); and B) frequency-dependent MS (χFD) against IRM_{1T}. Colors correspond to the intervals from which a given sample comes. Grayed areas correspond to samples clustering.

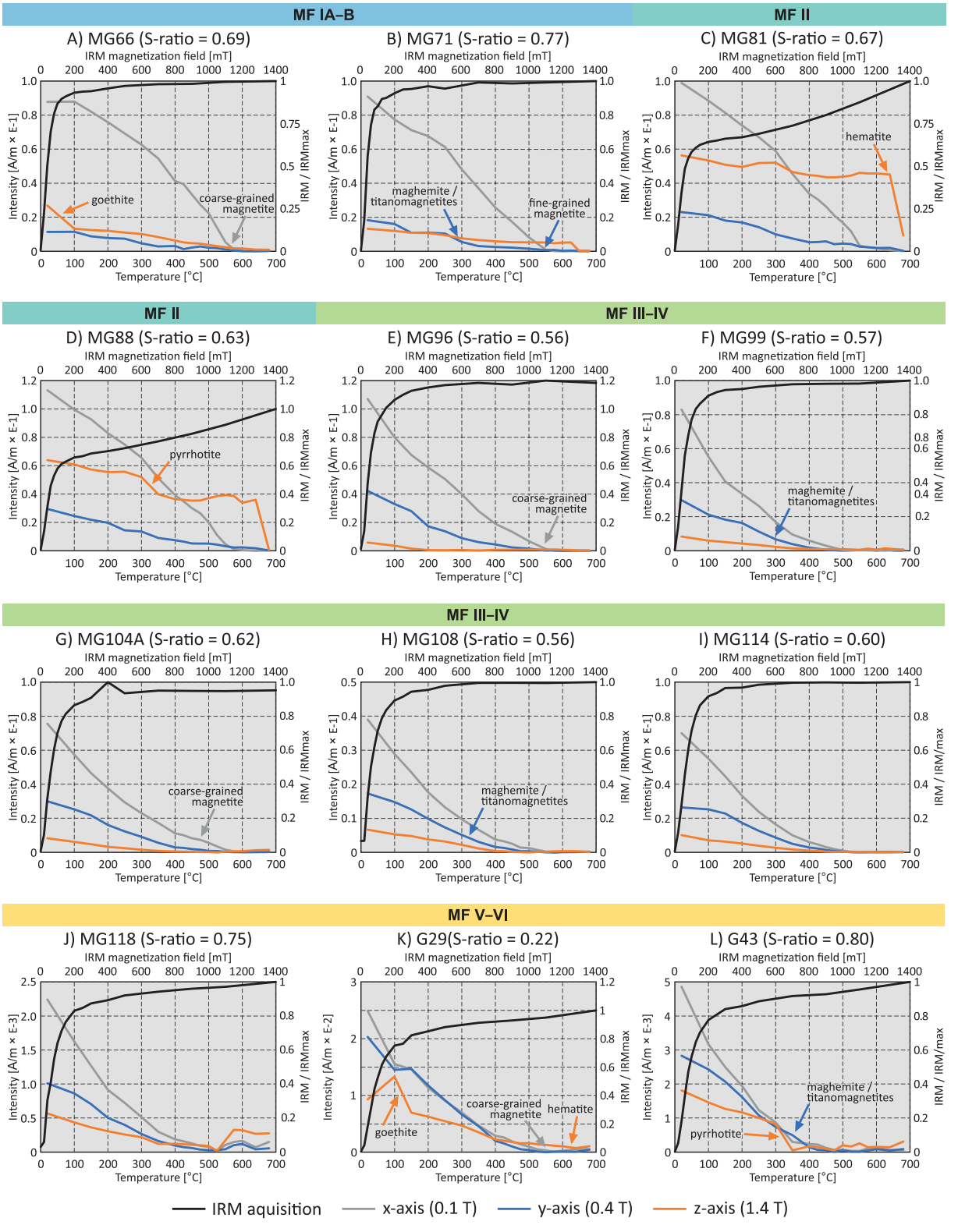

Text-fig. 6. Thermal demagnetization of the three-axis IRM and stepwise IRM acquisition curves of selected specimens from the Giewont series. Left Y-axis scale for three-axis IRM test curves, right Y-axis scale for IRM acquisition curve. Characteristic thermal demagnetization paths of selected minerals are indicated by arrows.

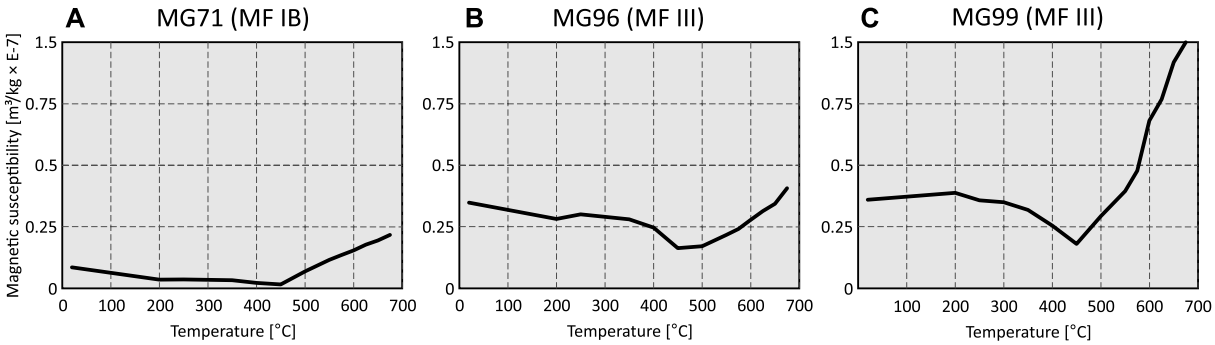

Text-fig. 7. Results of MS thermal dependence measurements. Note that the same Y-axis scale is used for each sample.

COEFFICIENTS OF DETERMINATION (R^2)

PEARSON CORRELATION COEFFICIENTS (PCC)

	Al	K	Rb	Ti	Ga	Zr	Th	Mn	Na	Mg	Zn	Ba	Ni	Co	V	Cu	P	U	Ca	
Al		0.97	0.96	0.94	0.90	0.90	0.84	0.62	0.56	0.27	0.25	0.22	0.06	0.06	0.05	0.05	0.00	0.04	0.21	Al
K	0.98		0.97	0.93	0.88	0.88	0.84	0.61	0.49	0.28	0.24	0.20	0.05	0.04	0.04	0.04	0.00	0.04	0.18	K
Rb	0.98	0.98		0.91	0.87	0.88	0.80	0.60	0.45	0.23	0.22	0.19	0.04	0.04	0.04	0.03	0.00	0.06	0.19	Rb
Ti	0.97	0.97	0.95		0.86	0.89	0.80	0.57	0.54	0.31	0.22	0.20	0.05	0.05	0.08	0.04	0.03	0.01	0.16	Ti
Ga	0.95	0.94	0.93	0.93		0.85	0.77	0.61	0.45	0.23	0.26	0.25	0.03	0.02	0.02	0.02	0.00	0.04	0.16	Ga
Zr	0.95	0.94	0.94	0.95	0.92		0.80	0.53	0.47	0.25	0.26	0.25	0.07	0.05	0.06	0.05	0.01	0.01	0.22	Zr
Th	0.91	0.92	0.89	0.89	0.88	0.90		0.54	0.44	0.24	0.20	0.29	0.05	0.04	0.03	0.04	0.00	0.05	0.20	Th
Mn	0.78	0.78	0.77	0.75	0.78	0.73	0.73		0.36	0.27	0.26	0.14	0.12	0.10	0.08	0.10	0.00	0.00	0.10	Mn
Na	0.75	0.70	0.67	0.74	0.67	0.68	0.67	0.60		0.56	0.29	0.10	0.12	0.17	0.11	0.10	0.00	0.01	0.02	Na
Mg	0.52	0.53	0.48	0.55	0.48	0.50	0.49	0.52	0.75		0.22	0.02	0.08	0.11	0.12	0.06	0.06	0.12	0.03	Mg
Zn	0.50	0.49	0.47	0.47	0.51	0.51	0.45	0.51	0.54	0.47		0.28	0.10	0.08	0.02	0.09	0.00	0.02	0.09	Zn
Ba	0.47	0.44	0.44	0.44	0.50	0.50	0.54	0.38	0.32	0.15	0.53		0.04	0.01	0.00	0.03	0.00	0.00	0.16	Ba
Ni	0.25	0.21	0.20	0.23	0.18	0.26	0.23	0.35	0.34	0.27	0.32	0.20		0.94	0.75	0.92	0.00	0.31	0.04	Ni
Co	0.24	0.21	0.20	0.23	0.14	0.22	0.21	0.32	0.42	0.33	0.29	0.11	0.97		0.80	0.92	0.00	0.30	0.01	Co
V	0.22	0.21	0.19	0.28	0.13	0.25	0.18	0.28	0.33	0.35	0.13	0.03	0.87	0.89		0.76	0.10	0.46	0.00	V
Cu	0.22	0.19	0.17	0.21	0.13	0.21	0.21	0.32	0.31	0.24	0.30	0.18	0.96	0.96	0.87		0.00	0.29	0.04	Cu
P	0.00	0.00	-0.02	0.17	0.05	0.09	-0.06	0.05	0.00	0.25	-0.02	-0.06	0.02	0.00	0.32	0.04		0.26	0.02	P
U	-0.20	-0.20	-0.24	-0.11	-0.20	-0.11	-0.22	-0.03	0.09	0.34	0.13	-0.07	0.55	0.55	0.68	0.54	0.51		0.12	U
Ca	-0.46	-0.42	-0.43	-0.40	-0.40	-0.46	-0.45	-0.31	-0.14	0.18	-0.29	-0.40	-0.19	-0.12	-0.05	-0.20	0.14	0.35		Ca
	Al	K	Rb	Ti	Ga	Zr	Th	Mn	Na	Mg	Zn	Ba	Ni	Co	V	Cu	P	U	Ca	

PEARSON CORRELATION COEFFICIENTS (PCC)

COEFFICIENTS OF DETERMINATION (R^2)

0.8 - 1 | 0.65 - 0.8 | 0.5 - 0.65

Table 1. Pearson correlation coefficients (PCC) and coefficients of determination (R2) for selected main and trace elements for combined Giewont and Mały Giewont sections.

Elemental geochemistry

Detrital input proxies

Due to its very limited diagenetic mobility, aluminum is adopted here as the main proxy for fine-grained lithogenic influx (see e.g., Tribovillard *et al.* 2006; van der Weijden *et al.* 2006). In order to evaluate the mutual relations between concentrations of selected main and trace elements, their Pearson correlation coefficients (PCCs) and coefficients of determination (R^2) have been calculated (Table 1). Based on their excellent correlation with Al, the elements K, Rb, Ti, Ga, Zr, and Th are regarded herein as detrital elements (see also e.g., Grabowski and Sobień 2015; Grabowski *et al.* 2021a); in addition, amongst the studied samples also Mn and Na have considerable detrital connotations.

Aluminum displays generally increasing concentrations through the Upper Kimmeridgian. It reaches its maximum content within the *Moluccana* dinocyst Zone (0.5%), followed by a decreasing uppermost Kimmeridgian–Upper Valanginian trend to, ultimately, less than 0.1%. Corresponding trends are observed in other – mentioned above – lithogenic elements (Text-fig. 8).

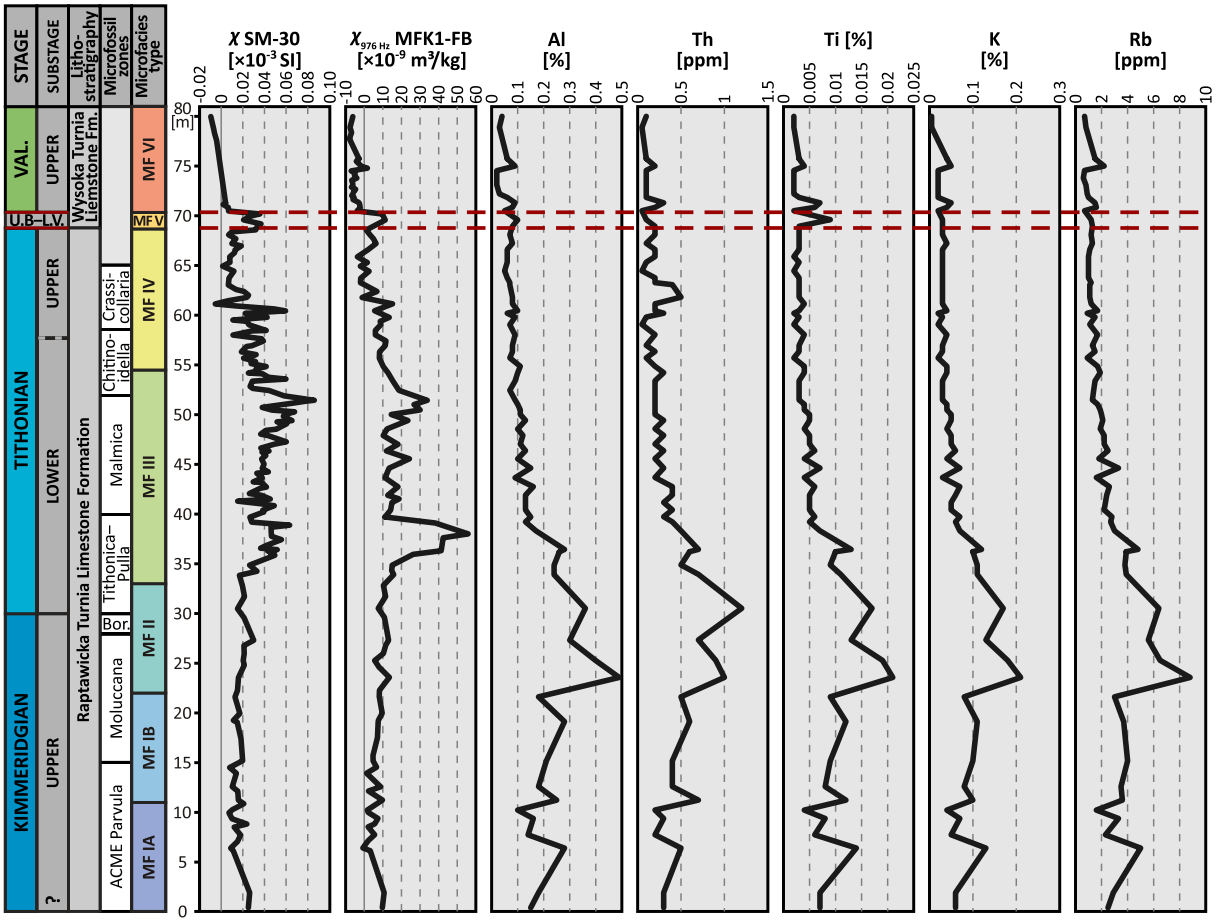

Text-fig. 8. Magnetic susceptibility (field and laboratory measured), Al, Th, Ti, K, and Rb laboratory-measured concentrations in the Upper Kimmeridgian–Upper Valanginian of the Giewont series. Abbreviations as on Text-fig. 4.

Redox proxies

Uranium concentrations do not correlate (or show even slightly negative correlation) with Al (Table 1), hence it is considered here as predominantly related to authigenic processes and carbonate fraction. In general, the studied sections are uranium-depleted (SOM 1). Consequently, almost no authigenic U is observed within the entire Kimmeridgian (Text-fig. 9). A major peak (to c. 3 ppm) characterizes the lowermost Tithonian beds (*Tithonica–Pulla* dinoflagellate Zone); above this peak, authigenic U decreases to slightly positive values, usually near or below 0.5 ppm. From the Upper Tithonian upwards an increasing trend is observed, which reaches its maximum (c. 3 ppm) within the Upper Berriasian–Lower Valanginian lithoclastic packstone (MF V); however, elevated values are also observed within the overlying Upper Valanginian encrinites (MF VI).

Corresponding trends are observed for the U/Th ratio, as well as in the Fe/Al ratio and the EF's of Mo and V (Text-fig. 9). Nonetheless, the lowermost Tithonian peak of U/Th is much less pronounced than in the case of authigenic U, while EF Mo depicts an interval of elevated values rather than a single peak. Interestingly, significant for redox interpretations may be also a cluster of elements with excellent mutual correlations (Ni, Co, V, Cu; Table 1). These are characterized by limited- to relatively-good correlation with U, while their EF's manifest similar trends as those described above, in particular the lowermost Tithonian peak (SOM 1).

Nutrient-type trace metals

Phosphorus does not reveal any statistical correlation with Al (and is relatively prone to U), whereas Ba and Zn correlate with the detrital fraction only limit-

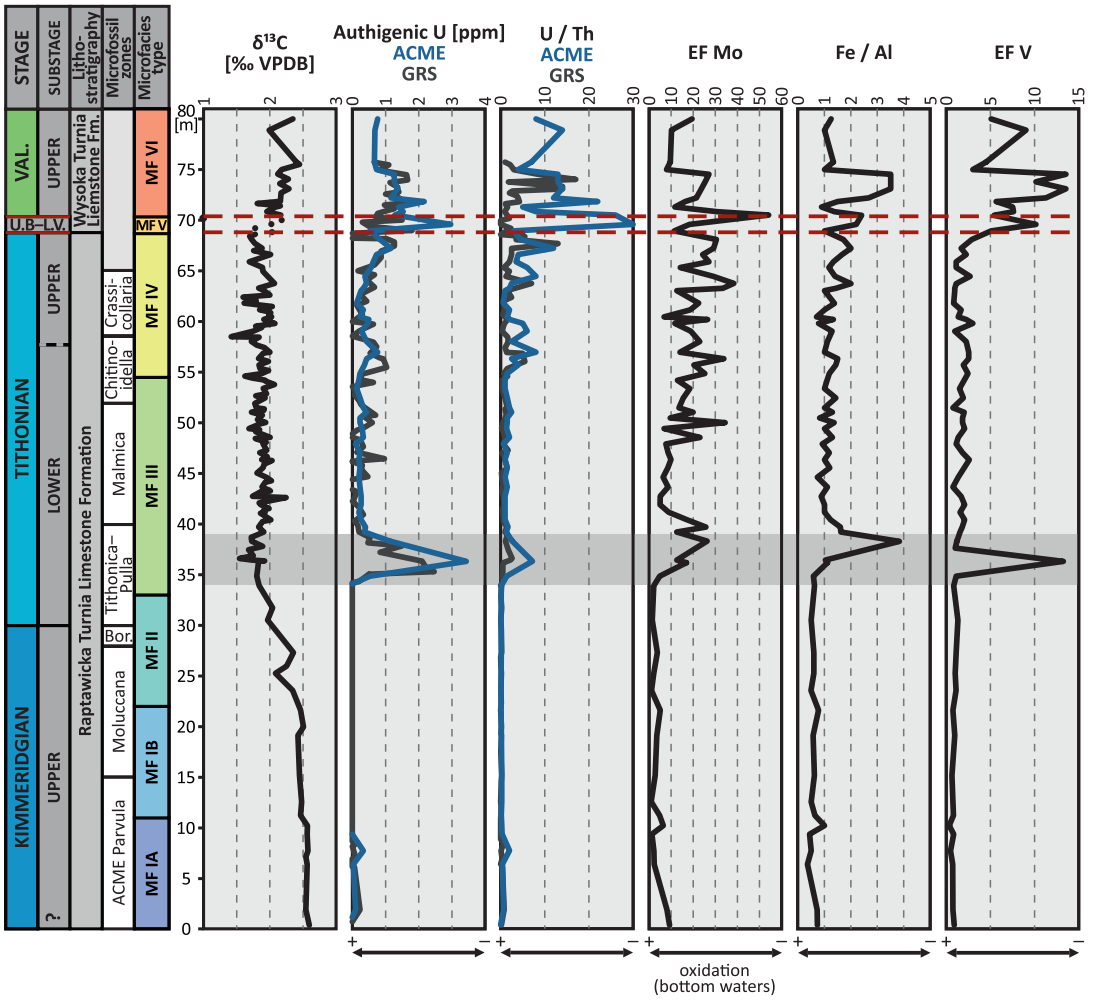

Text-fig. 9. Selected paleoredox proxies in the upper Kimmeridgian–upper Valanginian of the Giewont series. Gray belt indicates an lower Tithonian interval with a discernable environmental perturbation. Stable carbon isotope curve after Lodowski *et al.* (2022b). Abbreviations as on Text-fig. 4. ACME – data obtained in laboratory measurements; GRS – data obtained during field GRS measurements.

edly (Table 1). Nonetheless, only 'excess' concentrations of these elements are considered herein (Text-fig. 10; see also SOM 1). P_{EXCESS} content largely decreases through the Upper Kimmeridgian, is slightly elevated within the Lower Tithonian, and significantly increases in the Upper Berriasian–Lower Valanginian lithoclastic packstone (MF V) and Upper Valanginian encrinites (MF VI). Ba_{EXCESS} decreases slightly across the Kimmeridgian and depicts significantly increased concentrations above, within the lowermost Tithonian *Tithonica–Pulla* dinocyst Zone. In the overlying beds, Ba_{EXCESS} decreases to c. 4 ppm and remains stable above; however, another interval of – this time only slightly – elevated values is observed within the Upper Tithonian. Zn_{EXCESS} trends largely correspond to those of Ba_{EXCESS}, yet Zn_{EXCESS} reaches its minimum a bit lower, already within the Upper Kimmeridgian *Moluccana* dinocyst Zone.

Paleoclimate proxies

It may be observed that Zr/Al slightly increases across the Upper Kimmeridgian–lowermost Tithonian, and manifests a predominantly decreasing trend above; beyond these stratigraphic trends, perceptibly elevated values are observed within the *Crassicollaria* calpionellid Zone and within the lower part of MF VI (upper beds of the Giewont Member, upper Valanginian). The Al/K, in turn, decreases through the Upper Kimmeridgian, whereas a slightly increasing trend characterizes the Lower Tithonian. It is worth noting that significantly lowered Al/K is observed within the Upper Tithonian and the lower part

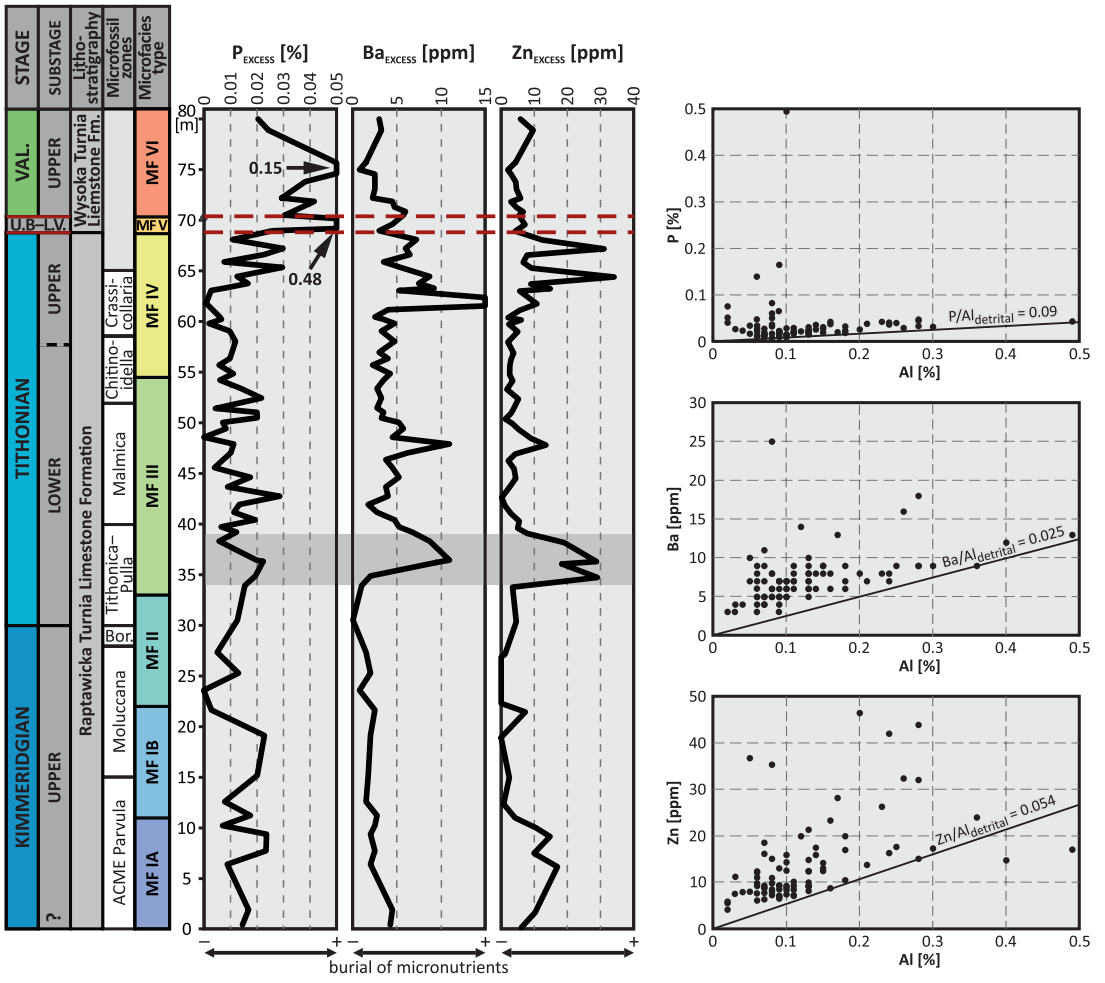

Text-fig. 10. Biological (excess) concentrations of selected paleoproductivity proxies in the upper Kimmeridgian–upper Valanginian of the Giewont series (left) and plots showing determination of their "detrital" constants (right; see also chapter MATERIALS AND METHODS). Gray belt indicates an interval of lower Tithonian environmental perturbation. Abbreviations as on Text-fig. 4.

of the Upper Valanginian (MF VI), while elevated ratios prevail in the MF V interval and the topmost part of the succession studied. The Chemical Index of Alteration (CIA) manifests comparable trends to those of Al/K, however its Upper Kimmeridgian part is not considered in this study due to the ambiguous record of Na concentrations (see SOM 1). Accordingly, relatively low CIA is characteristic of the middle part of the *Tithonica–Pulla* Zone (lowermost Tithonian); then it increases towards the *Malmica* dinocyst Zone and remains elevated up to the top of the Lower Tithonian. A sharp decline is observed within the *Crassicollaria* Zone, whereas elevated values are characteristic of the Upper Berriasian–Lower Valanginian (MF V). Finally, an abrupt drop (to ca 45%) accounts for the lower part of the MF VI interval (Upper Valanginian), whilst the top of the section is marked by equal abrupt rise of the CIA to elevated values. Ti/K shows predominantly decreasing values through the Upper Kimmeridgian–lowermost Tithonian, a trend which is terminated by a local positive peak in the lower part of the *Malmica* Zone. Above this peak, it remains stable up to the *Crassicollaria* Zone, yet within the topmost Tithonian beds an interval of lowered Ti/K may be noted; besides, Ti/K is characterized by a major peak in the MF V interval, lowered values in the lower part of the Upper Valanginian, and a significant increase at the top of the section, what corresponds well to CIA and Al/K. Intriguingly, Zr/Rb remain relatively stable through most of the section. However, local peaks are observed within the middle part of the MF IV and MF V intervals, whereas the lowest Zr/Rb are characteristic of the top of the section. Finally, Ti/Al shows some similarities to the Zr/Al curve: a local maximum

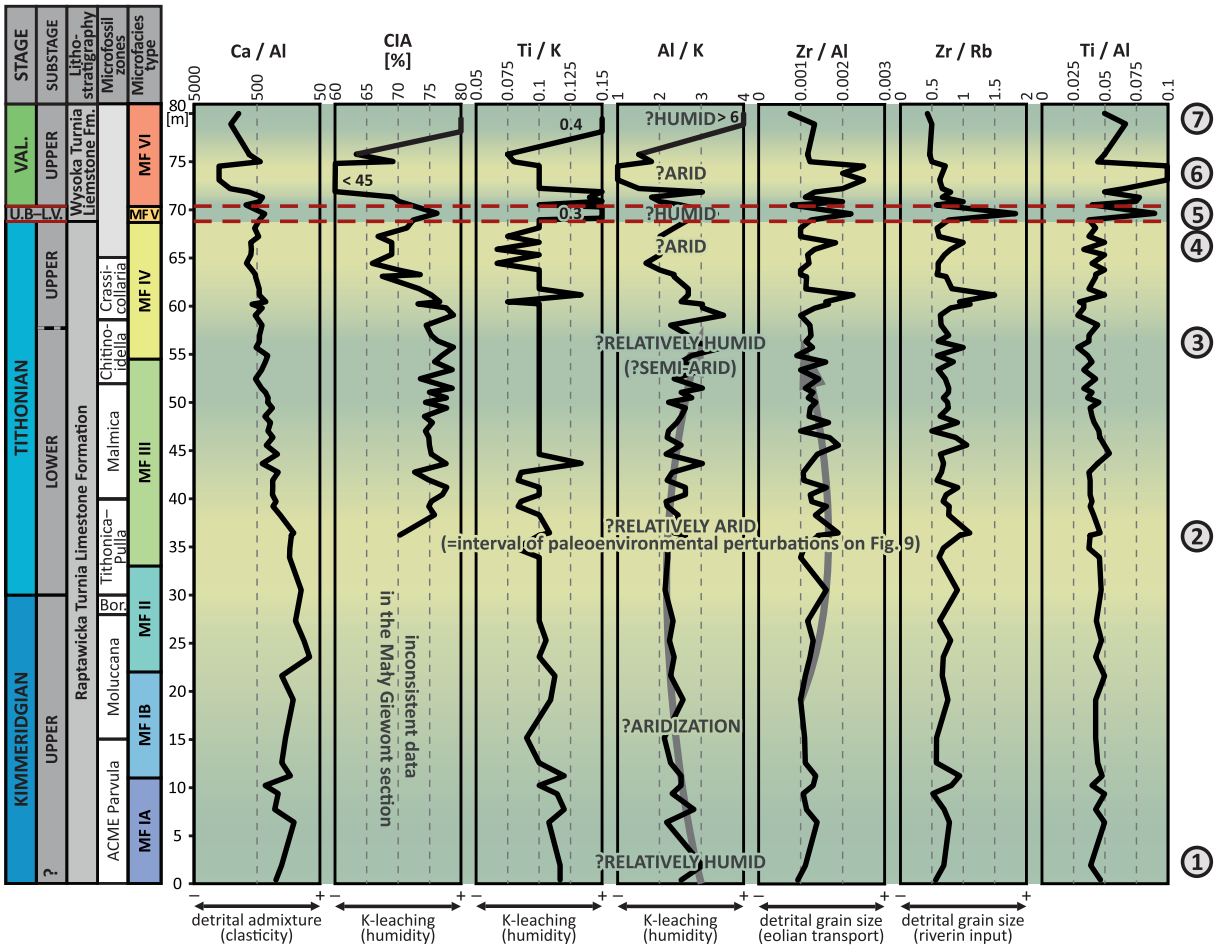

Text-fig. 11. Selected detrital- and weathering-related paleoenvironmental proxies in the upper Kimmeridgian–upper Valanginian of the Giewont series and their interpretation (color background). Note reverse logarithmic scale for Ca/Al. Gray arrows indicate trends. Abbreviations as on Text-fig. 4.

is observed within the middle part of the *Malmica* Zone, whereas a decreasing trend occurs above and continues up to the *Chitinoidella*/*Crassicollaria* zonal boundary. Within the Upper Tithonian a slightly increasing trend can be noted, whilst elevated values characterize the MF V interval (single peak) and lower part of the Upper Valanginian (Text-fig. 11).

INTERPRETATION

Sedimentary trends and events

Microfacies succession

Pszczółkowski *et al.* (2016) and Pszczółkowski (2018) discussed the autochthonous *vs.* allochthonous origin of the High-Tatric cyanoids and peloids, rejecting the latter solution (contrary to Lefeld and Radwański 1960). This implies that depths of sedimentation were constrained within the photic zone: that is, no more than 200 m below sea level (e.g., Sutton 2013), and most probably at "tens of meters" (Jenkyns 1972). This study adopts the above interpretation (Pszczółkowski 2018) and corroborates it with additional data.

Three major sedimentary trends/events are observed within the Upper Kimmeridgian–Valanginian microfacies succession of the Giewont series. Stratigraphically, these are: 1) the gradual disappearance of cyanoids through the Upper Kimmeridgian (MF IA–IB) and the onset of the pseudonodular limestone (note the lack of cyanoids) at the Kimmeridgian/Tithonian boundary interval (MF II); 2) the reappearance and dominance of cyanoids within the Tithonian (MF III–IV); and 3) the formation of an erosional

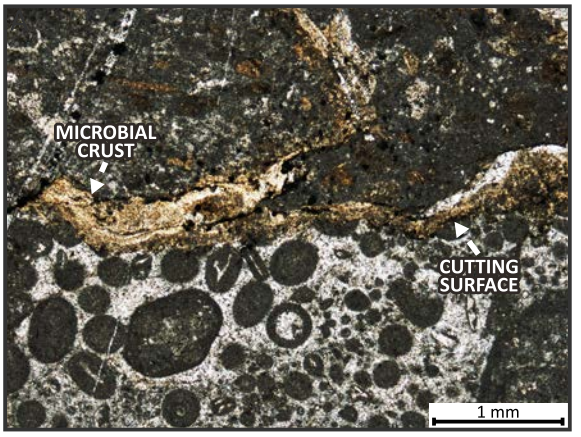

Text-fig. 12. Contact between the uppermost Tithonian cyanoid packstone (MF IV, lower) and the (?)Upper Berriasian–Lower Valanginian lithoclastic limestone (MF V, upper) in sample G29 (thin section) of the Giewont section. The cutting surface and a microbial crust are indicated by arrows.

gap on top of the Upper Tithonian cyanoid packstones (MF IV), covered by the (?)Upper Berriasian–Lower Valanginian lithoclastic packstone (MF V) and Upper Valanginian encrinites (MF VI; Text-figs 2 and 12). Here it is considered that the shallower the depth of the sea bottom, the higher the light penetration (understood here as the amount of light reaching the seafloor) and – putatively – the higher the environment energy (due to, for instance, wave energy). As a result, increasing light penetration is thought to favor the growth of cyanobacteria (therefore cyanoids; see also Murphy and Haugen 1985), while more turbulent environments should have resulted in upward rounding of coated grains. Consequently, in shallowing successions cyanoids should have trended towards progressively larger, more spherical shapes. As there is no literature data explaining morphologic variability of such small cyanoids as documented herein (all of them fall in the Type 1 grains of Védrine *et al.* 2007), the appearance of tangential internal structures and increasing grain sizes may document increasing energy of the environment, similarly to their closest analogue – ooids (e.g., Flügel 2010; Diaz and Eberli 2018; compare Text-fig. 3E and F).

Lodowski *et al*. (2022b) interpreted abundant dissolution seams and stylolites as indicative of an early-diagenetic (see Jenkyns 1974) origin of the pseudonodular texture (MF II) and estimated the latest Kimmeridgian–earliest Tithonian paleobathymetric setting of the Giewont series as deeper than 200 m, considerably beneath the base of the photic zone. Consequently, the gradual disappearance of cyanoids and onset of the pseudonodular limestone is considered to reflect the relative deepening of the Giewont series during the Late Kimmeridgian. Lodowski *et al*. (2022b) interpreted this phenomenon as resulting from a combination of vertical tectonic movements and eustasy; however, a possible relation between intensified clastic input (leading to cloudier water and a shallower photic zone) and the temporal vanishing of cyanoids was also noticed. Interestingly, although the model of Jenkyns (1974) requires very low sedimentation rates to form nodular structures, the sedimentation rates estimated in this study do not support occurrence of such conditions. Consequently, it is assumed that the conditions described by Jenkyns (1974) might have been only met to a limited extent, leading to superficial dissolution and the appearance of a pseudonodular texture, but not the development of a fully nodular structure.

Conversely, the disappearance of the pseudonodular limestone (MF II) within the lowermost Tithonian, coinciding with the reappearance and further ascendancy of cyanoids (MF III–IV), is interpreted as a manifestation of a shallowing trend (Lodowski *et al.* 2022b). Ultimately, the uppermost Tithonian–(?)Upper Berriasian erosional gap is thought to result from wave erosion and/or emersion (Lodowski *et al.* 2022b), and is thus indicative of a very shallow, or even (?temporarily) terrestrial paleoenvironment. Since such a dramatic paleobathymetric change (from more than 200 m during the earliest Tithonian to possible several meters during the Berriasian) could not have been related to the Tithonian–Berriasian regressive cycle alone (see Hardenbol *et al.* 1998; Hallam 2001, Haq 2014, 2018; Ray *et al.* 2019), Lodowski *et al*. (2022b), it can be suggested that tectonic uplift may have had a considerable influence.

The paleobathymetric interpretation of Lodowski *et al.* (2022b) can be additionally supported by the cyanoid morphometric results (Text-fig. 2), assuming the mechanism controlling their sizes and shapes proposed above. The Kimmeridgian trend of increasing depositional depth is evidenced by decreasing cyanoid abundance (= decreasing light penetration) and roundness (= decreasing environment energy) (MF IA–IB on Text-fig. 2). Conversely, the reappearance of cyanoids within the lowermost Tithonian (MF III) and the subsequent trend of increasing size and roundness (MF III–IV; Text-fig. 2) might point towards decreasing depths of the sea bottom (cf. Védrine *et al.* 2007). Even though a turbulent seafloor is not necessarily connected with shallow environments (e.g., Pomar *et al*. 2012) the trend of

shallowing seems undisputable (Lodowski *et al.* 2022b). Consequently, increasing roundness of cyanoids (note quite abrupt change in x/y ratio within the upper Lower Tithonian; Text-fig. 2) is considered herein as connected with decreasing depths of deposition, which enabled, eventually, storm waves to reach the seafloor. An additional factor that might have contributed to increasing cyanoid size (besides the shallowing-related increase in light penetration), was the decreased sedimentation rates during the Early–Late Tithonian. As microbial crusts grow slowly (e.g., Leinfelder *et al.* 1993), decelerated accumulation rates could have resulted in a thinner layer of mud covering coated grains (thus relatively better availability of the sunlight), which ensured prolonged growth and drove an increase in their average size.

The disconformity cutting the cyanoid packstone (MF IV / MF V boundary, Text-fig. 12) is covered by a thin "microbial crust". Subsequently, with the advent of open-marine conditions (either due to tectonic drowning and/or eustatic sea level rise), the lithoclastic packstones of MF V were deposited (Text-figs 2 and 3G). Nevertheless, another break in deposition likely occurred before the onset of Late Valanginian calcarenite sedimentation, as suggested by contrasting microfacies, rock magnetic perturbations, and a sudden drop in $\delta^{18}O$ values (Lodowski *et al.* 2022b).

Rock magnetism

In most cases, MS in carbonate rocks may be interpreted as a proxy of terrigenous admixture (e.g., Da Silva *et al.* 2015; Grabowski *et al.* 2017). Nevertheless, in the Giewont series a correlation between MS and the contribution of the clastic fraction is not obvious; for the entire studied succession, the PCC of Al and MS (laboratory measured) is only 0.3. However, when the succession is subdivided into five intervals of characteristic rock magnetic and/or detrital trends, that is: 1) an interval of increasing MS within MF I–II; 2) an interval of rock magnetic perturbations and elevated MS of MF III; 3) decreasing MS in MF IV; 4) elevated MS of the MF V interval; and 5) predominantly diamagnetic MF VI interval, their PCCs are 0.59, 0.09, 0.54, 1 (cf., only two datapoints), and 0.83, respectively. Consequently, the detrital connotations of MS are clearest in the Upper Kimmeridgian (MF I–II) and the Lower Cretaceous (MF V–VI) beds. Even if, to some extent, related to terrigenous input (PCC = 0.54), the decreasing MS within MF IV (Text-fig. 4) is considered as resulting from decreasing contribution of authigenic MS carriers, which clearly dominated the MF III interval below.

Accordingly, this phenomenon might relate to the appearance of superparamagnetic (ultra-fine grained) magnetite/maghemite. SP particles were found to occur within nearly the entire studied succession, and the relative loss of MS (% χ_{FD}) is rather stable, with mean 16% for the 15–60 m interval (the % χ_{FD} in the underlying and overlying intervals may be erroneous due to near-zero MS values) (Text-fig. 4). Noteworthy, MF I–II samples manifest an elevated ferromagnetic component, as document by increased values of IRM_{1T}, coinciding with low χ_{FD}. The opposite characterizes the MF III–IV interval (Text-fig. 4 and 5) – suggestive of predominantly superparamagnetic (= authigenic, see below) contribution to 'excess' MS.

As a consequence of the three-axis IRM experiments (Text-fig. 6), the decrease in the S-ratio within the basal Tithonian (lower part of MF III) is attributed to a relative increase in the contribution of medium-coercivity magnetite-type minerals, rather than hard fraction (hematite/goethite) abundance. Besides, the declining trend in S-ratio (Text-fig. 4) coincides with a sudden increase in the SP grains contribution. Consequently, the mineralogical change between MF II and MF III presumably resulted from the occurrence of the SP fraction and, the related, appearance of fine-grained (pseudo single-domain and/or single-domain) magnetite grains.

Additional data for rock magnetic interpretations come from the results of MS temperature dependence experiments. Pyrite is known to transform into magnetite and/or pyrrhotite above 450°C (e.g., van Velzen 1992; Li and Zhang 2005; Waters *et al.* 2008), causing a significant rise in MS above this temperature. This phenomenon is, indeed, observed within the Giewont series (Text-fig. 7); moreover, MS in the Lower Tithonian sample MG99 (meter 40.6; Text-fig. 7C) increases much more than in the Upper Kimmeridgian sample MG71 (meter 12.1; Text-fig. 7A), which suggests that the amount of pyrite also increases. Although there is no continuous record of pyrite presence, it is noteworthy that the occurrence of this sulfide coincides well with redox proxies (e.g., EF Mo and authigenic U, Text-fig. 9), which point towards an interval of oxygen depletion initiating at the very same stratigraphic horizon – lowermost part of MF III interval (see chapter *Paleoredox and paleoproductivity proxies*).

Taking the above into consideration, it is concluded that the MS in the Upper Kimmeridgian is largely driven by lithogenic input, while the magnetic mineralogy of the MF III–IV interval was more strongly affected by diagenetic processes. Grabowski

et al. (2009) suggested that SP magnetite in the Valanginian of the Zliechov succession in the Stražov Mts (CWC, Slovakia) may have been derived from a late diagenetic (synthrusting) oxidation of pyrite and subsequent precipitation of magnetite; such an interpretation may also be applicable for the Giewont series. The maghemite documented from the MF III–IV interval (Text-fig. 6) also might have originated during the late-diagenetic oxidation of magnetite (Sidhu *et al.* 1977; Jackson and Swanson-Hysell 2012). Finally, late diagenetic processes affected the Tithonian portion of the succession to a much greater extent than in the Upper Kimmeridgian. This phenomenon might be related either to the availability of pyrite (i.e., the subject of oxidation) and/or the microfacies succession.

Lithogenic input and sedimentation rates

Low observed concentrations of detrital elements (Al, Th, K, and Rb on Text-fig. 8) confirm that the Giewont series was exposed to a very limited supply of fine-grained siliciclastic sediments. Raw geochemical data distinguish two intervals with distinct lithogenic influx trends: 1) the Upper Kimmeridgian, characterized by increasing detrital element concentrations; and 2) the Tithonian–Upper Valanginian, where a secular decline in detrital element content is observed. However, the entire Upper Kimmeridgian–Tithonian interval is characterized by most probably decreasing sedimentation rates (from c. 10 m/My in MF I to 6.5 m/My in MF IV – see chapter *Sedimentation rates*), which must have inevitably resulted in an apparent enrichment of the detrital fraction. This assumption is based on the fact, that – in geological record – the combination of stable lithogenic influx and decelerating rates of deposition (= carbonate accumulation) manifests in a trend of increasing clasticity (i.e., increasing Al content). Consequently, the Late Kimmeridgian is interpreted as a time of relatively stable or, at most, only slightly intensifying lithogenic influx, whereas the actual decrease in terrigenous input during the Tithonian was likely stronger than suggested by the raw geochemical record.

Paleoredox conditions vs. deposition of nutrient-style trace metals

The redox proxies examined in this study are characterized by positive peaks of their values in the lowermost Tithonian and elevated (relative to the Upper Kimmeridgian) values above (Text-fig. 9). Even though authigenic U and U/Th have relatively low values (compare Text-fig. 9 with Jones and Manning 1994), Algeo and Liu (2020) assert that the redox framework of Jones and Manning (1994) should not be directly applied to other formations without taking into account local sedimentary factors. Accordingly, the occurrence of pyrite (Text-fig. 7) in association with extraordinarily high EF Mo and Fe/Al (Text-fig. 9) may indicate that, during the Tithonian, the sediment-water interface in the study area was subject to reducing conditions (see also see also Berner 1984 and Algeo and Liu 2020).

It is of considerable importance to determine whether fluctuations in micronutrient contributions actually reflect changes in surface (paleo)productivity, or rather result from other sedimentary and/or oceanographic processes. Accordingly, the upper Kimmeridgian is characterized by relatively low and declining Ba_{EXCESS} and Zn_{EXCESS} (Text-fig. 10), which could be interpreted as corresponding to efficient uptake of micronutrients – hence relatively high surface productivity, or as depicting rather low (and decreasing) productivity, if it is assumed that productive elements were predominantly subjected to burial processes (e.g., due to stratification). In this context, the positive trends observed in detrital element concentrations (Al, Th, Ti, K, and Rb on Text-fig. 8) are suggestive of intensifying lithogenic influx – hence, an increasing nutrient supply. Consequently, irrespective of the state of the water column (mixed *vs.* stratified), relatively high clastic input should result in enhanced surface productivity.

In addition, the discovery of an oxygen-deficient interval within the Tithonian (c. 34–39 m of the Giewont composite section; see above) has profound consequences for the interpretation of trace metal concentrations. The sudden increase in Ba_{EXCESS} and Zn_{EXCESS} (and, to some extent, P_{EXCESS}; Text-fig. 10) in the lowermost Tithonian correlates well with major redox proxy peaks (Text-fig. 9). Moreover, as the entire upper Kimmeridgian–Tithonian exhibits continuously decreasing sedimentation rates, the exceptional concentrations of both paleoredox proxies and trace metals are thought to represent an actual increase in their burial rates (i.e., their peak contributions most likely do not result from relative condensation). As no increase in lithogenic element concentrations is observed within the interval (compare Text-figs 8–10), this phenomenon must have been related to perturbations in the local/regional marine circulation system. This, in turn, might have led not only to (?)partial stratification, limited vertical transportation of dissolved O_2, and – eventually – benthic oxygen deficiency (as suggested by redox proxies),

but also to increased burial fluxes of P, Ba, and Zn, which were no longer subjected to biologic recycling due to reduced water column mixing and the slowdown of the nutrient shuttle (cf. Falkowski 2012).

Both Ba_{EXCESS} and Zn_{EXCESS} decrease immediately above their lowermost Tithonian peaks; however, they remain slightly elevated in relation to the Upper Kimmeridgian beds, as do the redox proxies. Another increase in their concentrations is observed within the Upper Tithonian, yet another interval in which various redox proxies depict relatively high values (compare Text-figs 9 and 10); these might have been driven by comparable mechanisms of fixation and enrichment as during the earliest Tithonian. As the Tithonian is characterized by increasing cyanoid abundance (Text-fig. 2), at least limited water circulation must have taken place (during storms, for instance), such that rotation of coated grains was ensured.

Finally, although the Upper Kimmeridgian–Tithonian P_{EXCESS} exhibits more ambiguous trends than Ba_{EXCESS} and Zn_{EXCESS}, some similarities are present: in particular, a decreasing trend within the Upper Kimmeridgian and elevated values in the Lower Tithonian (Text-fig. 10). The absence of a well pronounced peak in the lowermost Tithonian may result from oxygen depletion and related P-escape processes (i.e., via diffusion of bacterially regenerated PO_4^{3-} to the water column; e.g., Tribovillard *et al.* 2006).

Paleoclimate proxies

Interpretation of the K-related paleoclimate proxies (CIA, Al/K, Ti/K) is not straightforward and must be taken with caution, since relative variations in K content might be connected either with the kaolinite/illite proportions (where an increase in Al/K indicates a relative increase in kaolinite, thus strengthened chemical weathering and humid paleoclimate; e.g., Schneider *et al*. 1997; Calvert and Pedersen 2007; Tian *et al*. 2011), or with the illite/smectite ratio (where low K suggests the presence of smectite, hence arid conditions; e.g., Diester-Haass *et al*. 1993; Niebuhr 2005). Considering that K-depletion indicates chemical weathering, variations in K-related proxies (CIA, Ti/K, Al/K on Text-fig. 11) could be interpreted as resulting from: 1) humid early Late Kimmeridgian; 2) arid earliest Tithonian; 3) Early/Late Tithonian humidification; 4) Late Tithonian aridization; 5) humid (?)Late Berriasian–Early Valanginian; 6) arid early Late Valanginian; and 7) humid Late Valanginian (see Text-fig. 11). Besides, second-order climate fluctuations might also have occurred, as evidenced i.e., by minor elevation of Ti/K and Al/K within the lower part of the *Malmica* dinocyst zone, and/or their variations near the *Chitinoidella*/*Crasicollaria* zonal boundary. The reverse scenario, starting with an arid early Late Kimmeridgian and humid Kimmeridgian/Tithonian transition, should be applied when considering the smectite-related concept (Diester-Haass *et al*. 1993; Niebuhr 2005). Both interpretative frameworks are discussed below, with special attention paid to their implications for correlations over regions.

DISCUSSION

Relative variation of K content – indications of humid/arid conditions?

Integration of geochemical data (stable carbon and oxygen isotope ratios, $^{87}Sr/^{86}Sr$), changes in nannoplankton communities and sea-level variations allowed Price *et al.* (2016) to provide an outline of the western Tethyan climate evolution during the latest Jurassic–earliest Cretaceous. The authors come to the conclusion, that from the Late Kimmeridgian onwards the climate began to gain in aridity, with a climax of this process during the Tithonian/Berriasian transition, whereas a consecutive trend of humidification characterized the Berriasian–Early Valanginian (i.e., Abbink *et al*. 2001; Rameil 2005; Bover-Arnal and Strasser 2013; Morales *et al*. 2013). Nonetheless, these general trends appear to have been disrupted by other, second-order climate perturbations.

In this context, the lowermost Tithonian *Tithonica–Pulla* dinocyst Zones can be compared with the *Hudlestoni* ammonite Zone of northern Europe. This assumption relies on the fact that the *Tithonica–Pulla* dinocyst zones roughly correspond to the M22n magnetozone, as do the *Hybonotum–Semiforme* Tethyan ammonite Zones (Grabowski *et al*. 2019; fig. 12 in Lodowski *et al*. 2022b). Within their stratigraphic range, in turn, falls the *Hudlestoni* ammonite Zone of the Sub-Boreal realm (Wierzbowski *et al*. 2017; Turner 2018). Consequently, both the lowermost Tithonian minimum in Al/K and CIA, and maximum in Zr/Al (Text-fig. 11) can be stratigraphically correlated with the arid '*Hudlestoni* event' of northern Europe (e.g., Abbink *et al*. 2001; Hesselbo *et al*. 2009; Turner and Huggett 2019). It may be noted, that the Kimmeridgian/Tithonian minimum in Al/K correlates with the lowermost Tithonian peaks in redox proxies (compare Text-figs 9 and 11), which point to the state of the bottom waters hypoxia. This suggests stratification of water masses, associated herein with

the onset of an arid climate mode, with respect to the mechanism in which weakened monsoonal atmospheric circulation (= arid type) reduces the efficiency of Ekman transport, limiting the mixing of the water column. Consequently, the lowermost Tithonian (elevated redox proxies on Text-fig. 9) is expected to have been deposited under arid climate conditions. Additionally, the corresponding trends in Al/K and Zr/Al also point to progressive aridization during the Kimmeridgian/Tithonian transition (Hesselbo *et al*. 2009; van der Hoeven 2022). Due to that, the scenario of chemical weathering driven K-depletion is favoured here as best explaining the relative variations in K content. Here it must be also emphasized, that the relation between climate change and paleoredox conditions discussed in this study is different to, and cannot be compared to, conditions driving the Mesozoic anoxic events (i.e., Jenkyns 1999). Basically, sediments considered herein were subjected only to oxygen depletion, but definitely not to strongly reducing (anoxic/euxinic) conditions. Based on it, the mechanism of greenhouse driven OAE's (Jenkyns 1999) should not be applied in this case; instead, all observations can be explained by the alternative model of aridification-related stratification of the water column and seafloor hypoxia.

Somewhat problematic is the issue of the subsequent mid-Tithonian humidification, which is manifested by increasing Al/K and CIA, as well as decreasing Zr/Al within the *Chitinoidella* dinocyst Zone (Text-fig. 11). So far, humid pulses during the mid-Tithonian have been recognized only in northwest France (Deconinck *et al.* 1983), England (Hesselbo *et al*. 2009), and the Polish Basin (Grabowski *et al*. 2021a), but their correlation is not well constrained. In the case of the western Tethyan sections, traces of mid-Tithonian humidification might be followed in the Lókút succession of the Transdanubian Range (Grabowski *et al.* 2017). There, a sharp increase in the relative abundances of the genus *Watznaueria* near the base of magnetozone M20n, combined with the temporal disappearance of *Nannoconus*, may point to increased fertility of surface waters, hence a better mixed water column (e.g., due to monsoonal upwelling; see also Erba 1994, Giraud *et al.* 2016).

A relatively short-lasting arid phase characterized the early Late Valanginian; the climate became more balanced soon after, at the transition between the *Verrucosum* and *Peregrinus* ammonite Zones (Duchamp-Alphonse *et al*. 2011; Kujau *et al*. 2013; Westerman *et al*. 2013). Importantly, a paleoclimate interpretation based on the K-leaching mechanism corresponds well with the scenario described above (Text-fig. 11). It might be correlated to the "arid phase" (6) in the lower part of the Upper Valanginian of the Giewont series. The overlying sediments indicating "humid phase" (7) might correspond to a phase of seasonal climate (Duchamp-Alphonse *et al*. 2011; Charbonnier *et al.* 2020) in the *Peregrinus* and *Furcillata* zones of the Upper Valanginian. It must be noted, that although the geochemical data obtained from the MF V interval may be biased by the geochemistry of lithoclasts, it is considered that these are younger than the top of MF IV, and therefore may provide reliable data on the paleoenvironmental evolution since the Late Tithonian. This assumption relies on the fact, that the lithoclasts do not resemble any of the studied substrate rocks, hence they are thought to represent reworked material from the Lower (?and partly Upper) Berriasian, which is now missing (Lodowski *et al*. 2022b).

Lithogenic influx and its controls

As discussed in the subchapter *Lithogenic input*, the High-Tatric area was subjected to a relatively weak, and presumably slightly increasing, lithogenic influx during the Late Kimmeridgian and a continuous decrease in clastic supply during the Tithonian. Among the Late Jurassic environmental trends and events that could have resulted in such a record, climate change (i.e., progressive aridization) is considered to be the most comprehensive solution, however, the possible effects of eurybatic variations and Late Jurassic tectonic activity must also be treated (see below).

One of the important sedimentary trends observed within the Giewont series is the decreasing contribution of the terrigenous fraction through the Tithonian. It is intriguing to note that a decline in lithogenic influx is observed within the Tithonian of numerous Western Tethyan successions, for example in the Lower Sub-Tatric (Grabowski *et al*. 2013), the Pieniny Klippen Belt (Grabowski *et al*. 2019; cf. Michalík *et al*. 2016), and the Transdanubian Range (Grabowski *et al*. 2017; Lodowski *et al*. 2022a), as well as in southern England (cf. Morgans-Bell *et al*. 2001) and in the Polish Basin (Grabowski *et al*. 2021a) (Text-fig. 13). Climate aridization was put forth to explain decreasing clastic supply in all of these localities; it was additionally supported by clay mineral analysis (e.g., Hesselbo *et al*. 2009). These observations render the decline in siliciclastic input of supra-regional importance, supporting the Late Kimmeridgian–Early Berriasian climate perturbations as a key factor affecting lithogenic influx in

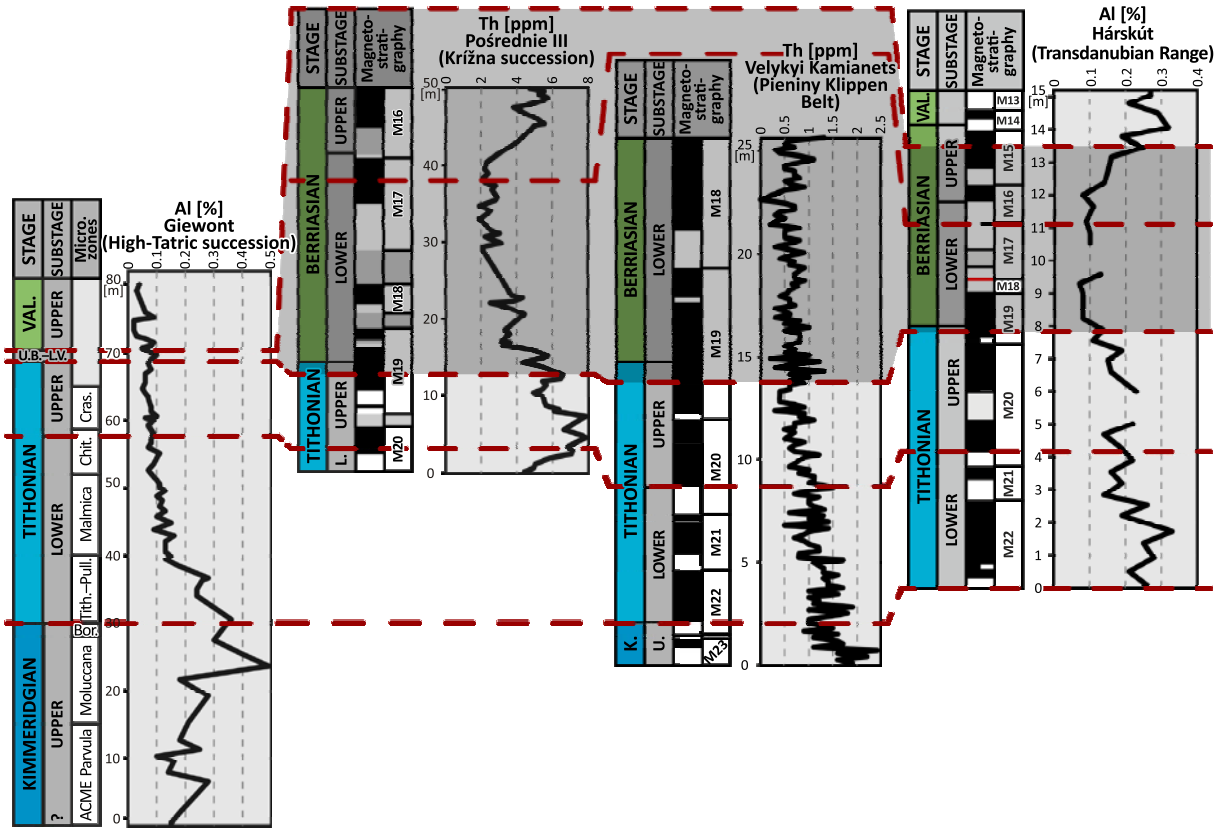

Text-fig. 13. Correlation of lithogenic influx proxies between the Giewont (High-Tatric, this study), Pośrednie III (Lower Sub-Tatric, Grabowski *et al.* 2013), Velykyi Kamianets (Pieniny Klippen Belt, Grabowski *et al.* 2019), and Hárskút (Transdanubian Range, Lodowski *et al.* 2022) sections. Approximated range of the uppermost Tithonian–lower Berriasian erosional gap in the High-Tatric succession (grayed out area) is indicated. Abbreviations: K. – Kimmeridgian; VAL. – Valanginian.; U.B.–L.V. – Upper Berriasian–Lower Valanginian; L. – Lower; U. – Upper; Tith.–Pull. – Tithonica–Pulla; Bor. – Borzai; Chit. – Chitinoidella; Cras. – Crassicollaria.

both Tethyan and Boreal Europe. In this scenario, the general trend of aridization might have been interrupted by minor periods of humidification, such as the mid-Tithonian one (Text-fig. 11).

Nevertheless, it must be remembered that the above-mentioned climatic effect might have been additionally strengthened by other important controls. For instance, a common correlation between decreasing clasticity and a major global regression (Hardenbol *et al.* 1998; Haq 2014) is observed both in western Tethyan (e.g., Grabowski *et al.* 2013, 2017, 2019, 2021a; Michalík *et al.* 2016; Lodowski *et al.* 2022a) and Boreal (Morgans-Bell *et al.* 2001) successions. In turn, even though multiple tectonic processes related to the progressive closure of the western parts of the Neotethys Ocean influenced the structure of western Neotethyan basins and resultant Late Jurassic–Early Cretaceous sedimentation patterns (e.g., Gawlick *et al.* 1999; Csontos and Vörös 2004; Schmid *et al.* 2008 and references therein), it seems that none of the tectonic phenomena controlled the Late Kimmeridgian–Tithonian lithogenic input to the South Tatric Ridge. One of the pivotal tectonic events was the formation of the Neotethyan Collision Belt (NCB), a chain of accretionary wedges and ophiolites ranging from the Hellenides to the Western Carpathians (Text-fig. 1; e.g., Missoni and Gawlick 2011). In the Western Carpathians, traces of the NCB can be followed in the flysch and mélange facies of the Meliaticum. While accretionary wedges already began to develop there during the late Middle Jurassic (Plašienka 2018; Putiš *et al.* 2019), there is no precise stratigraphic data on its latest Jurassic evolution. Gawlick *et al.* (2015) concluded that in the Northern Calcareous Alps erosion of an obducted ophiolite stack started during the Early Kimmeridgian, whereas Steiner *et al.* (2021) discussed the Late Kimmeridgian–Early Tithonian unroofing of the NCB. This tectonism may have re-

sulted in elevated rates of erosion, driving increased lithogenic input to neighboring sedimentary basins, as observed in the upper Kimmeridgian of the High-Tatric zone. However, the distribution of siliciclastic detritus was restricted by the development of nearby carbonate platforms (located to the N/NW from the collision zone, e.g., Plassen Carbonate Platform; Gawlick and Schlagintweit 2006); these did not ultimately drown until the late Berriasian. The rather limited uplift of the NCB may have not been enough to directly affect the High-Tatric depositional zone; if present, this effect likely was very restricted. In addition, Tatricum was located much further to the NE (in relation to the Plassen Platform), whereas the South Tatric Ridge was additionally separated from the 'NCB zone' by the Zliechov Basin, which received a significant portion of its lithogenic input from the NCB during the Tithonian (2–3% of Al, Grabowski *et al.* 2013). As such, it is considered that the lithogenic supply to the Giewont series might have been largely contributed by eolian transport.

Tracing Late Kimmeridgian–Valanginian sedimentary controls in the High-Tatric succession

The Late Kimmeridgian–earliest Tithonian: a "monsoonal upwelling" control?

Numerous studies point to a possible link between upwelling, climate, and facies distribution in the Jurassic and Cretaceous of the Western Tethys (e.g., Golonka and Krobicki 2001; Hotinski and Toggweiler 2003; Muttoni *et al*. 2005; Rais *et al.* 2007; De Wever *et al.* 2014; Michalík *et al.* 2017; Bąk and Bąk 2018). Since the abundance of radiolarians is linked with nutrient-rich surface waters, increased sedimentation of their silicious tests should result from elevated nutrient supply (e.g., De Wever *et al.* 2001, 2014; Baumgartner 2013). According to De Wever *et al*. (2014), a key mechanism controlling the surface productivity of Mesozoic and Cenozoic oceans was monsoon-driven upwelling. Golonka and Krobicki (2001) discussed the possibility of an upwelling regime in the Pieniny Klippen Belt; they concluded that the prevailing wind direction during the Late Jurassic and Early Cretaceous was parallel to the axis of the Czorsztyn Ridge (from southwest to northeast; Alpine/Atlantic Tethys), and therefore might have been favorable for the induction of upwelling on its southern rim. Since the South Tatric Ridge was presumably parallel to the Czorsztyn Ridge (Text-fig. 1), here it is assumed that the model of Golonka and Krobicki (2001) can also be adopted for the neighboring High-Tatric deposition zone.

The Upper Kimmeridgian of the Giewont series is characterized by slightly decreasing concentrations of nutrient-style trace metals and stable (or only slightly increasing) lithogenic influx (Text-fig. 14). This record corresponds well with the sedimentary turnover that took place in the Zliechov Basin, that is a switch from siliceous to carbonate dominated deposition. Although radiolarites do not occur in the Jurassic of the High-Tatric succession (High-Tatric *sensu stricto*, see Plašienka and Ožvoldová 1996 and compare with Lefeld *et al.* 1985), they are typical of the Middle–Upper Jurassic deposits of the Zliechov Basin. There, they disappear within the Upper Kimmeridgian, overlain by uppermost Kimmeridgian–Tithonian carbonates (Jach *et al.* 2012, 2014; Jach and Reháková 2019). This process was roughly coeval with both the beginning of the climate aridization interval (see above) and the start of the general trend of decreasing $\delta^{13}C$ signatures (Cramer and Jarvis 2021). As the onset of the arid climate was concurrent with oxygen depletion at the seafloor, it is presumed that a diminished monsoon weakened the mechanism of monsoonal upwelling, resulting in reduced water column mixing and stratification. Accordingly, a decreasing supply of nutrients due to progressively weakening upwelling might have been an important factor driving the radiolarian decline during the latest Jurassic (see also discussion in DeWever *et al.* 2014; for discussion on the Late Jurassic radiolarites from the Zliechov Basin see Jach and Reháková 2019). Such a correlation allows the presumption, that changes in the efficiency of monsoonal upwelling might have controlled trophic conditions prevailing in the High-Tatric deposition zone (see also Michalík *et al.* 2017). Here, the 'river plumes' mechanism of Baumgartner (2013) is unlikely to apply due to the fact, that increased concentrations of nutrient-style trace metals do not correlate with lithogenic proxies (compare Text-figs 8 and 10).

Weissert and Channell (1989) discussed the possibility that general climate aridization during the Tithonian might have decreased the amount of material transferred from continents to oceans, thus decelerating marine productivity, reducing marine organic matter burial rates (i.e., organic carbon) and, eventually, causing lighter $\delta^{13}C$ signatures. A significant decrease in $\delta^{13}C$ (by c. 1‰ VPDB) within the uppermost Kimmeridgian–lowermost Tithonian of the Giewont series (Text-figs 9 and 14), is thought to document a corresponding scenario, yet with aridization driving the stratification and progressive weakening of the nutrient shuttle system.

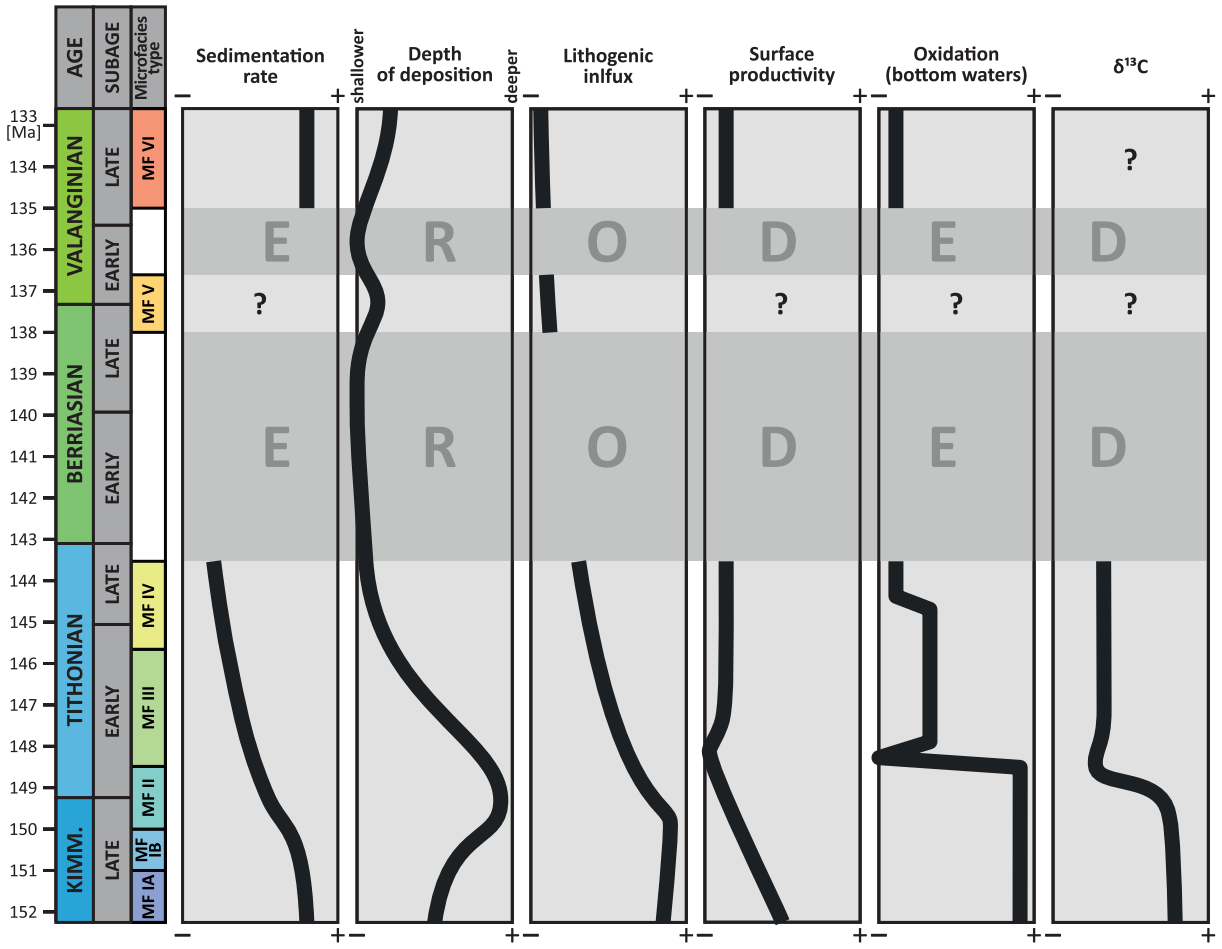

Text-fig. 14. Generalized sedimentary trends during the Late Kimmeridgian–Valanginian, as interpreted for the High-Tatric deposition zone. Abbreviations: KIMM. – Kimmeridgian.

Tithonian: regional trends vs. local sedimentary controls

As suggested by Weissert and Erba (2004; see also discussion above), carbon cycling during the Tithonian resulted from a long-term evolution of the paleoenvironment, which eventually led to relatively high water pH (relative to the Oxfordian–Kimmeridgian) and low organic to carbonate carbon burial ratios (C_{ORG}/C_{CARB}): conditions favoring biocalcification. This is in agreement with observations in the sedimentary successions of the Western Carpathians, that is the entirely carbonate Tithonian of the High-Tatric, Križna, and Pieniny Klippen Belt successions (e.g., Birkenmajer 1963, 1975). However, there are some – apparently insignificant – differences in the stable carbon isotope records that they yield.

The Tithonian of the Giewont series records relatively low and stable $\delta^{13}C$ values (Text-fig. 9), whereas a progressive decrease is usually observed in other western Tethyan successions (e.g., fig. 13 in Lodowski *et al.* 2022b, see also Cramer and Jarvis 2020). Consequently, it is assumed that in the High-Tatric deposition zone, carbon cycling during the Tithonian was dependent not only on regional (?global) oceanographic conditions, but also on local sedimentary controls, the most likely being depth of deposition (Text-fig. 14). In this case, the abundance of cyanobacteria (i.e., cyanoids), in conjunction with relatively poorly mixed water column during the Tithonian, might have resulted in a local seawater deficit in ^{12}C, shifting $\delta^{13}C$ to relatively heavier values than in more basinal areas. Additionally, cyanobacteria are thought to be the primary drivers of C_{ORG} export, driving the conditions limiting biocalcification (note the decelerated sedimentation rates during the Late Tithonian; Text-fig. 14) and favoring oxygen depletion at the seafloor (Text-figs 9 and 14).

When considering paleodepths of the South Tatric Ridge it must be noted, that besides eustatic sea-level changes, these might have been affected also by block-tilting. The Jurassic–Cretaceous transition in the Osobita massif (Western Tatra Mts, Slovakia) is characterized by the occurrence of volcanic rocks and carbonate breccia (Lefeld *et al*. 1985; Staniszewska and Ciborowski 2000; Madzin *et al*. 2014). According to Madzin *et al*. (2014), volcanism (interpreted by the authors as connected with rifting and opening of the North Penninic-Magura Ocean) was already evident during the Late Tithonian, lending credibility to the assumption that the paleobathymetry of the High-Tatric area was related to both the Tithonian regression and local tectonics.

Late Berriasian–Valanginian sedimentary controls

Volcanic activity in the Osobita massif increased, reaching its maximum during the Late Berriasian–?Early Valanginian (Madzin *et al.* 2014). This drove the uplift of the South Tatric Ridge, eventually leading to the (?)emergence and erosion of the youngest strata, as manifest in the Giewont series in the uppermost Tithonian–Berriasian disconformity (see also Lodowski *et al.* 2022b). It is intriguing that a similar phenomenon has also been reported not only from the High-Tatric autochthonous sedimentary cover (Grabowski *et al*. 2022), but also from the Manín Unit (Michalík and Vašíček 1987; Michalík *et al*. 2005; Michalík *et al*. 2012), which is usually interpreted as having originated on the southern slopes of the South Tatric Ridge (e.g., Plašienka 2019). Finally, traces of the South Tatric Ridge erosion can be followed in the Zliechov and Hlboč sections (both deposited in the Zliechov Basin), in which Berriasian breccias were described by Michalík *et al.* (1995, see also Michalík 2007).

The timing of uplift in the High-Tatric area corresponds well with the late Berriasian tectonic reactivation in the Neotethyan Collision Belt (Missoni and Gawlick 2011). Outside of the Northern Calcareous Alps, this event is expressed by increased lithogenic supply in the CWC (Grabowski and Sobień 2015), Southern Alps (Goričan *et al.* 2018), Transdanubian Range (Fodor *et al.* 2013; Lodowski *et al.* 2022a), Western Balkans (Grabowski *et al.* 2016, 2021b), and – to some extent – the Northern Apennines (increasing magnetic susceptibility, Satolli and Turtù 2016). Also the facies development (including hiatuses) and brachiopod fauna of the Pieniny Klippen Belt document Tithonian–Berriasian uplift (Birkenmajer 1986; Krobicki 1994), however there it is associated with rifting and opening of the North Penninic-Magura Ocean during the Walentowa rifting phase (Berriasian–Hauterivian; Plašienka 2012; see also Oszczypko *et al*. 2012). Related also to the tectonic extension interpretation are the plate basalts of the Belice succession (Soták *et al.* 1993; Plašienka 2003), the Osobita massif basanites (Madzin *et al*. 2014), and the volcanic rocks of the Mecsek Mts (Tisza Mega-Unit; see Haas and Péró 2004; Szederkényi *et al*. 2013). Consequently, the uplift of the High-Tatric can be considered as connected with both the subduction in the NCB and rifting in the Penninic oceans, supporting the idea of a geodynamic connection between these two processes (see Plašienka, 2003).

A massive (?)Upper Berriasian–Lower Valanginian P_{EXCESS} peak (MF V; c. 20 times higher in concentration than in the underlying beds; Text-fig. 10) is interpreted here as associated with upwelling-related accumulation of phosphates. The predominantly humid Late Berriasian–Early Valanginian climate (e.g., Föllmi 2012; Morales *et al*. 2013; Westermann *et al.* 2013) favored monsoonal upwelling, which conceivably provided an efficient P-supply from deeper parts of the basin (compare with Brandano *et al.* 2016). Elevated values of redox proxies within both the Upper Berriasian–Lower Valanginian and the Upper Valanginian beds (Text-fig. 9) point to oxygen depletion at the seafloor. This phenomenon may be related to the decreased solubility of oxygen in warmer water, as has been proposed for Late Devonian Upper Kellwasser event (e.g., Bond *et al.* 2013). The Upper Valanginian redox peaks might have resulted from another interval of arid climate and related stratification (compare Text-figs 9 and 11), what is in concordance with literature data (e.g., Föllmi 2012; Westermann *et al*. 2013). That being said, a cause and effect relationship between climate mode (arid, characterized by presumably low atmospheric energy *vs.* humid, monsoon type), state of the water column (stratified or mixed, respectively) and accumulation of nutrient-style trace metals can be used to explain sedimentary conditions

Text-fig. 15. Schematic reconstruction of the major High-Tatric events during the Kimmeridgian–Valanginian. Stratigraphic framework as in → Lodowski *et al.* (2022b; modified). Timescale after Ogg (2020). Major and 2nd order eustatic cycles with respect to Hardenbol *et al.* (1998) and Haq (2014, 2018). Climate reconstruction for the Giewont series is based on this study, supplemented by Abbink *et al.* (2001), Hesselbo *et al.* (2009), Föllmi (2012), Grabowski *et al.* (2017; 2021b). Paleobathymetry of the Giewont series is approximate. Abbreviations: Praetin. – Praetintinnopsella; Moluc. – Moluccana; K_2 – Late Kimmeridgian; T_1 – Early Tithonian; T_2 – Late Tithonian; B_2 – Late Berriasian; V_2 – Late Valanginian. Climate log: green–humid; yellow – arid.

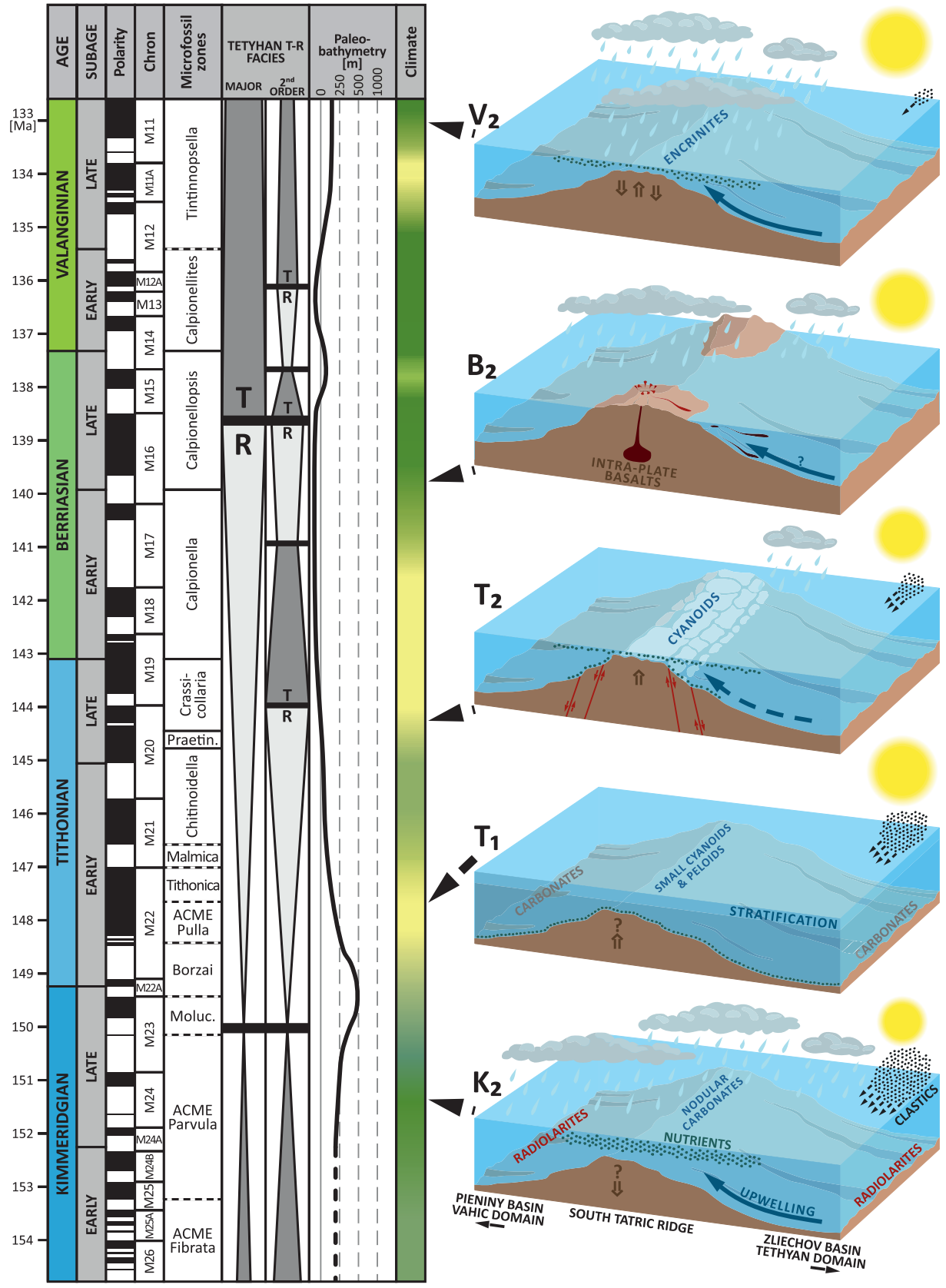
AGE
SUBAGE
Polarity
Chron
Microfossil zones
TETYHAN T-R FACIES
MAJOR
2nd ORDER
Paleo-bathymetry [m]
0
250
500
1000
Climate
133 [Ma]
134
135
136
137
138
139
140
141
142
143
144
145
146
147
148
149
150
151
152
153
154
VALANGINIAN
BERRIASIAN
TITHONIAN
KIMMERIDGIAN
LATE
EARLY
M11
M11A
M12
M12A
M13
M14
M15
M16
M17
M18
M19
M20
M21
M22
M22A
M23
M24
M24A
M24B
M25
M25A
M26
Tintinnopsella
Calpionellites
Calpionellopsis
Calpionella
Crassi-collaria
Praetin.
Chitinoidella
Malmica
Tithonica
ACME Pulla
Borzai
Moluc.
ACME Parvula
ACME Fibrata
T
R
V2
ENCRINITES
B2
INTRA-PLATE BASALTS
T2
CYANOIDS
T1
CARBONATES
SMALL CYANOIDS & PELOIDS
STRATIFICATION
CARBONATES
K2
RADIOLARITES
NODULAR CARBONATES
NUTRIENTS
CLASTICS
RADIOLARITES
UPWELLING
PIENINY BASIN
VAHIC DOMAIN
SOUTH TATRIC RIDGE
ZLIECHOV BASIN
TETHYAN DOMAIN

prevailing the High-Tatric deposition zone not only during the Late Kimmeridgian–Tithonian, but also the earliest Cretaceous.

CONCLUSIONS

This study presents the results of sedimentologic, rock magnetic, and geochemical investigations in the Upper Kimmeridgian–Upper Valanginian of the Giewont series. The collected data was interpreted in terms of their paleoenvironmental significance and discussed with regards to local and regional paleoclimate, paleoecology, and the tectonic framework. The High-Tatric deposition zone is presumed to have been affected by numerous latest Jurassic–earliest Cretaceous paleoenvironmental perturbations recognized in the western Tethyan and Subboreal realms. Nevertheless, its isolated paleogeographic setting, in conjunction with the impact of local tectonic controls, resulted in clearly distinct sedimentary conditions and evolution relative to neighboring successions (see also Text-fig. 15).

A significant increase in the terrigenous contribution during the Late Kimmeridgian (Al, Th, Ti, K, and Rb on Text-fig. 8) is interpreted as being only apparent, depicting in fact relatively stable (or slightly increasing?) lithogenic influx under decreasing sedimentation rates (Text-fig. 14). In turn, the Tithonian trend of decreasing clastic supply is correlated with similar phenomena observed in western Tethyan and northern Europe successions (Text-fig. 13); it is thought to result from a switch to an arid climate mode during the latest Kimmeridgian–Early Tithonian, which eventually led to lowered rates of continental erosion. Beyond these observations, this study supports the utility of the MS as a convenient and valuable proxy for estimating clastic input, even in paleogeographically isolated areas such as the High-Tatric. However, special attention must be paid to potential diagenetic overprints as observed, for instance, within the Lower Tithonian beds, where late-diagenetic oxidation resulted in significant changes in magnetic mineralogy, the appearance of superparamagnetic minerals, and disruption of the detrital-associated MS record (Text-fig. 8).

The results of cyanoid morphometry (size and roundness measurements) suggest the applicability of this method for considerations of paleodepths. The greatest depositional depths in the High-Tatric succession are expressed through the occurrence of the pseudonodular limestones of the Kimmeridgian–Tithonian boundary interval. Tectonic uplift, combined with sea-level fall, resulted in the Tithonian shallowing trend, as evidenced by the microfacies succession and cyanoid morphometry (their bigger size and more spherical shape; Text-fig. 2). Progressive shallowing eventually led to wave erosion (or even emersion?), as shown by the disconformity spanning the uppermost Tithonian–(?)Upper Berriasian (Text-fig. 12). The stratigraphic range of this hiatus corresponds well with both the beginning of the Walentowa rifting phase and the tectonic reactivation in the Neotethyan Collision Belt, which supports Plašienka's (2003) model for the geodynamic relation between subduction in the Meliata Ocean and rifting in the Penninic Realm.

Although somehow ambiguous, the paleoclimate proxy record (CIA, Al/K, Ti/K, Zr/Al; Text-fig. 11) documented from the Giewont series is in agreement with data both from other western Tethyan successions and from northwest Europe. This suggests a supra-regional significance of these latest Jurassic–earliest Cretaceous climate changes, that is that the common (at least to some extent) scenario of paleoclimate evolution might have affected the vast part of Europe, ranging from southern England and the Polish Basin to the north and the Vocontian Basin and the Central Western Carpathians to the south. Of particular importance is the temporal Early Tithonian arid period known from northwest Europe (the "*Hudlestoni* event") and a similar phenomenon documented in the High-Tatric succession.

The association between intervals characterized by exceptionally high oxygen depletion and increased trace metal concentrations (lowermost Tithonian, Upper Tithonian, cf. lower part of the Upper Valanginian) is interpreted as resulting from enhanced burial of these elements during periods of water stratification. Such conditions occurred during arid climate modes – then monsoons were diminished, limiting the induction of monsoonal upwellings, hence restricting mixing of the water column (Text-fig. 15).

Acknowledgements

These investigations were financially supported by the National Science Center, Poland (projects nos.: 2016/21/B/ST10/02941 and 2011/03/B/ST10/05256; leader: J. Grabowski; PGI-NRI, Warsaw). The authors would like to express their warmest thanks to Jordan Todes (Department of Geophysical Sciences, University of Chicago) for linguistic consultations, and the reviewers of this manuscript for their kind remarks and general influence on its final form: PhD Leona Chadimová

(Institute of Geology, Czech Academy of Sciences, Czech Republic), PhD Constantin Balica (Department of Geology, Babeș-Bolyai University in Cluj Napoca, Romania), and PhD Roman Aubrecht (Faculty of Natural Sciences, Comenius University in Bratislava, Slovakia).

REFERENCES

Abbink, O., Targarona, J., Brinkhuis, H. and Visscher, H. 2001. Late Jurassic to earliest Cretaceous palaeoclimatic evolution of the southern North Sea. *Global and Planetary Change*, **30**, 231–256.

Algeo, T.J. and Li, C. 2020. Redox classification and calibration of redox thresholds in sedimentary systems. *Geochimica et Cosmochimica Acta*, **287**, 8–26.

Algeo, T.J. and Liu, J. 2020. A re-assessment of elemental proxies for paleoredox analysis. *Chemical Geology*, **540**, 119549.

Bassetti, M.-A., Berné, S., Sicre, M.-A., Dennielou, B., Alonso, Y., Buscail, R., Jalali, B., Hebert, B. and Menniti, C. 2016. Holocene hydrological changes in the Rhône River (NW Mediterranean) as recorded in the marine mud belt. *Climate of the Past*, **12**, 1539–1553.

Baumgartner, P.O. 2013. Mesozoic radiolarites – Accumulation as a function of sea surface fertility on Tethyan margins and in ocean basins. *Sedimentology*, **60**, 292–318.

Bąk, K. and Bąk, M. 2013. Foraminiferal and radiolarian biostratigraphy of the youngest (Late Albian through Late Cenomanian) sediments of the Tatra massif, Central Western Carpathians. *Acta Geologica Polonica*, **63**, 223–237.

Bąk, M. and Bąk, K. 2018. Palaeoceanographic regime during the Oxfordian–Kimmeridgian in the Western Tethys recorded by radiolarian assemblages in the siliceous sediments of the Pieniny Klippen Belt, Carpathians. *Geological Journal*, **54**, 3362–3375.

Berner, R.A. 1984. Sedimentary pyrite formation: An update. *Geochimica et Cosmochimica Acta*, **48**, 605–615.

Birkenmajer, K. 1963. Stratigraphy and palaeogeography of the Czorsztyn series (Pieniny Klippen Belt, Carpathians) in Poland. *Studia Geologica Polonia*, **10**, 1–380.

Birkenmajer, K. 1975. Tectonic control of sedimentation at the Jurassic–Cretaceous boundary in the Pieniny Klippen Belt, Carpathians. *Mémoires du Bureau de Recherches Géologiques et Minières*, **86**, 294–299.

Birkenmajer K. 1977. Jurassic and Cretaceous lithostratigraphic units of the Pieniny Klippen Belt, Carpathians, Poland. *Studia Geologica Polonica*, **45**, 1–158.

Birkenmajer, K. 1986. Stages of structural evolution of the Pieniny Klippen Belt, Carpathians. *Studia Geoogica Polonica*, **88**, 7–32.

Bond, D.P.G., Zatoń, M., Wignall, P.B. and Marynowski, L. 2013 Evidence for shallow-water 'Upper Kellwasser' anoxia in the Frasnian–Famennian reefs of Alberta, Canada. *Lethaia*, **46**, 355–368.

Bover-Arnal, T. and Strasser, A. 2013. Relative sea-level change, climate, and sequence boundaries: insights from the Kimmeridgian to Berriasian platform carbonates of Mount Saléve (E France). *International Journal of Earth Sciences*, **102**, 493–515.

Brandano, M., Westphal, H., Mateu-Vicens, G., Preto, N. and Obrador, A. 2016. Ancient upwelling record in a phosphate hardground (Tortonian of Menorca, Balearic Islands, Spain). *Marine and Petroleum Geology*, **78**, 593–605.

Bureau Veritas Minerals Schedule of Service & Fees. 2020. https://commodities.bureauveritas.com/sites/g/files/zypfnx241/files/media/document/Metals%20Minerals%20and%20Environmental_2020_Fee_%20Schedule_MINING_CAD.pdf

Calvert, S.E. and Pedersen, T.F. 2007. Elemental Proxies for Palaeoclimatic and Palaeoceanographic Variability in Marine Sediments: Interpretation and Application. *Developments in Marine Geology*, **1**, 567–644.

Casellato, C.E. 2009. Causes and consequences of calcareous nannoplankton evolution in the Late Jurassic: implications for biogeochronology, biocalcification and ocean chemistry. Ph.D. Thesis, Universita degli Studi di Milano, Milano, 122 pp.

Casellato, C.E. and Erba, E. 2021. Reliability of calcareous nannofossil events in the Tithonian–early Berriasian time interval: Implifications for a revised high resolution zonation. *Cretaceous Research*, **117**, 104611.

Cecca, F., Fourcade, E. and Azéma, J. 1992. The disappearance of the "Ammonitico Rosso". *Palaeogeography, Palaeoclimatology, Palaeoecology*, **99**, 55–70.

Charbonnier, G. Duchamp-Alphonse, S., Deconinck, J.-F., Adatte, T., Spangenberg, J.E., Colin, C. and Föllmi, K.B. (2020) A global palaeoclimatic reconstruction for the Valanginian based on clay mineralogical and geochemical data. *Earth-Science Reviews*, **202**, 103092.

Cramer, B.D. and Jarvis, I. 2020. Carbon Isotope Stratigraphy. In: Gradstein, F.M., Ogg, J.G., Schmitz, M.D. and Ogg, G.M. (Eds), The Geologic Time Scale 2020, 955–1022. Elsevier; Amsterdam, London, Cambridge.

Csontos, L. and Vörös, A. 2004. Mesozoic plate tectonic reconstruction of the Carpathian region. *Palaeogeography, Palaeoclimatology, Palaeoecology*, **210**, 1–56.

Da Silva, A.C., Whalen, M.T., Hladil, J., Chadimova, L., Chen, D., Spassov, S., Boulvain, F. and Devleeschouver, X. 2015. Magnetic susceptibility application: a window onto ancient environments and climatic variations: foreword. *Geological Society, London, Special Publications*, **414**, 1–13.

De Wever, P., Dumitrica, P., Caulet, J.P., Nigrini, C. and Caridroit, M. 2001. Radiolarians in the Sedimentary Record, 533 pp. Gordon and Breach Science Publications, London.

De Wever, P., O'Dogherty, L. and Goričan, Š. 2014. Monsoon as a cause of radiolarite in the Tethyan realm. *Comptes Rendus Geoscience*, **346**, 287–297.

Dearing, J.A., Dann, R.J.L., Hay, K., Lees, J.A., Loveland, P.J.,

Maher, B.A. and O'Grady, K. 1996. Frequency-dependent susceptibility measurements of environmental materials. *Geophysics Journal International*, **124**, 228–240.

Deconinck, J.-F., Chamley, H., Debrabant, P. and Colbeaux, J.P. 1983. Le Boulonnais au Jurassique supérieur: données de la minéralogie des argiles et de la géochimie. *Annales de la Société Géologique du Nord*, **102**, 145–152.

Diaz, M.R. and Eberli, G.P. 2018. Decoding the mechanism of formation in marine ooids: A review. *Earth-Science Reviews*, **190**, 536–556.

Diester-Haass, L., Robert, C. and Chamley, H. 1993. Paleoceanographic and paleoclimatic evolution in the Weddell Sea (Antarctica) during the middle Eocene–late Oligocene, from a coarser sediment fraction and clay mineral data (ODP Site 689). *Marine Geology*, **114**, 233–250.

Duchamp-Alphonse, S., Fiet, N., Adatte, T. and Pagel, M. 2011. Climate and sea-level variations along the northwestern Tethyan margin during the Valanginian C-isotope excursion: Mineralogical evidence from the Vocontian Basin (SE France). *Palaeogeography, Palaeoclimatology, Palaeoecology*, **302**, 243–254.

Erba, E. 1994. Nannofossils and superplumes, the early Aptian "nannoconid" crisis. *Paleoceanography*, **9**, 483–501.

Falkowski, P. 2012. The power of plankton. *Nature*, **483**, 17–20.

Flügel, E. 2010. Microfacies of Carbonate Rocks. Analysis, Interpretation and Application, 984 pp. Springer; Heidelberg, Dordrecht, London, New York.

Fodor, L., Sztanó, O. and Kövér, S. 2013. Mesozoic deformation of the northern Transdanubian Range (Gerecse and Vértes Hills). *Acta Mineralogica-Petrographica*, **31**, 1–52.

Föllmi, K.B. 2012. Early Cretaceous life, climate and anoxia. *Cretaceous Research*, **35**, 230–257.

Gawlick, H.-J. and Schlagintweit, F. 2006. Berriasian drowning of the Plassen carbonate platform at the type-locality and its bearing on the early Eoalpine orogenic dynamics in the Northern Calcareous Alps (Austria). *International Journal of Earth Sciences*, **95**, 451–462.

Gawlick, H.-J., Frisch, W., Vecsei, A. Steiger, T. and Böhm, F. 1999. The change from rifting to thrusting in the Northern Calcareous Alps as recorded in Jurassic sediments. *Geologische Rundschau*, **87**, 644–657.

Gawlick, H.-J., Aubrecht, R., Schlagintweit, F., Missoni, S. and Plašienka, D. 2015. Ophiolitic detritus in Kimmeridgian resedimented limestones and is provenance from an eroded obducted ophiolitic nappe stack south of the Northern Calcareous Alps (Austria). *Geologica Carpathica*, **66**, 473–487.

Giraud, F., Mattioli, E., López-Otálvaro, G., Lécuyer, C., Suchéras-Marx, B., Marineau, F., Arnaud-Godet, F. and de Kænel, E. 2016. Deciphering processes controlling mid-Jurassic coccolith turnover. *Marine Micropaleontology*, **125**, 36–50.

Golonka, J. and Krobicki, M. 2001. Upwelling regime in the Carpathian Tethys: a Jurassic–Cretaceous palaeogeographic and plaeoclimatic perspective. *Geological Quarterly*, **45**, 15–32.

Goričan, Š, Žibret, L., Košir, A., Kukoč, D. and Horvat, A. 2018. Stratigraphic correlation and structural position of Lower Cretaceous flysh-type deposits in the eastern Southern Alps (NW Slovenia). *International Journal of Earth Sciences*, **107**, 2933–2953.

Grabowski, J. and Sobień, K. 2015. Variation in clastic input in the Berriasian of the Lower Sub-Tatric (Krížna) succession in the Tatra Mountains (Central Western Carpathians, Poland): data from magnetic susceptibility and inorganic geochemistry. *Annales Societatis Geologorum Poloniae*, **85**, 139–150.

Grabowski, J., Michalík, J., Szaniawski, R. and Grotek, I. 2009. Sythrusting remagnetization of the Krížna nappe: high resolution palaeo- and rock magnetic study in the Strážovce section, Strážovské vrchy Mts, Central West Carpathians (Slovakia). *Acta Geologica Polonica*, **59**, 137–155.

Grabowski, J., Schnyder, J., Sobień, K., Koptíkova, L., Krzemiński, L., Pszczółkowski, A., Hejnar, J. and Schnabl, P. 2013. Magnetic susceptibility and spectral gamma logs in the Tithonian–Berriasian pelagic carbonates in the Tatra Mts (Western Carpathians, Poland): Palaeoenvironmental changes at the Jurassic/Cretaceous boundary. *Cretaceous Research*, **43**, 1–17.

Grabowski, J., Lakova, I., Petrova, S., Stoykova, K., Ivanova, D., Wójcik-Tabol, P., Sobień, K. and Schnabl, P. 2016. Paleomagnetism and integrated stratigraphy of the Upper Berriasian hemipelagic succession in the Barlya section Western Balkan, Bulgaria: Implications for lithogenic input and paleoredox variations. *Palaeogeography, Palaeoclimatology, Palaeoecology*, **461**, 156–177.

Grabowski, J., Haas, J., Stoykova, K., Wierzbowski, H. and Brański, P. 2017. Environmental changes around the Jurassic/Cretaceous transition: New nannofossil, chemostratigraphic and stable isotope data from the Lókút section (Transdanubian Range, Hungary). *Sedimentary Geology*, **360**, 54–72.

Grabowski, J., Bakhmutov, V., Kdýr, Š., Krobicki, M., Pruner, P., Rehákova, D., Schnabl, P., Stoykova, K. and Wierzbowski, H. 2019. Integrated stratigraphy and palaeoenvironmental interpretation of the Upper Kimmeridgian to Lower Berriasian pelagic sequences of the Velykyi Kamianets section (Pieniny Klippen Belt, Ukraine). *Palaeogeography, Palaeoclimatology, Palaeoecology*, **532**, 109216.

Grabowski, J., Chmielewski, A., Ploch, I., Rogov, M., Smoleń, J., Wójcik-Tabol, P., Leszczyński, K. and Maj-Szeliga, K. 2021a. Palaeoclimatic changes and inter-regional correlations in the Jurassic/Cretaceous boundary interval of the Polish Basin: portable XRF and magnetic susceptibility study. *Newsletters on Stratigraphy*, **54**, 123–158.

Grabowski, J., Stoykova, K., Wierzbowski, H. and Wójcik-Tabol, P. 2021b. Upper Berriasian chemostratigraphy, clay minerals and calcareous nannofossils of the Barlya section (Western Balkan, Bulgaria): implications for paleoclimate and productivity changes, and stratigraphic correlations across the Alpine Tethys. *Palaeogeography, Palaeoclimatology, Palaeoecology*, **567**, 110252.

Grabowski, J., Bąk, K., Bąk, M., Krobicki, M., Lodowski, D., Uchman, A., Golonka, J., Górny, Z., Hejnar, J., Iwańczuk, J., Olszewska, B., Oszczypko, N., Salata, D., Wierzbowski, A. and Wójcik-Tabol, P. 2022. From shallow to deep marine depositional environments of the Cretaceous northwestern Tethys – a record of alpine system differentiation in the Polish Carpathians. In: Walaszczyk, I.P. and Todes, J. (eds) Cretaceous of Poland: Field Guides, 11th International Cretaceous Synposium, Warsaw, Poland, 2022. 297–362, Faculty of Geology, University of Warsaw.

Haas, J. and Péró, C. 2004. Mesozoic evolution of the Tisza Megaunit. *International Journal of Earth Sciences*, **93**, 297–313.

Hallam, A. 2001. A review of the broad pattern of Jurassic sea-level changes and their possible causes in the light of current knowledge. *Palaeogeography, Palaeoclimatology, Palaeoecology*, **167**, 23–37.

Haq, B.U. 2014. Cretaceous eustasy revisited. *Global and Planetary Change*, **113**, 44–58.

Haq, B.U. 2018. Jurassic sea-level variations: A reappraisal. *GSA Today*, **28**, 4–10.

Hardenbol, J., Thierry, J., Harley, M.B., Jacquin, Th., de Graciansky, P.-C. and Vail, P.R. 1998. Mesozoic and Cenozoic sequence chronostratigraphic framework of European basins. Appendix. *SEPM Special Publication*, **160**, 763–786.

Häusler, H., Plašienka, D. and Polák, M. 1993. Comparison of Mesozoic successions of the Central Eastern Alps and the Central Western Carpathians. *Jahrbuch der Geologischen Bundesanstalt*, **136**, 715–739.

Hesselbo, S.P., Deconinck, J.-F., Huggett, J.M. and Morgans-Bell, H.S. 2009. Late Jurassic palaeocolimatic change from clay mineralogy and gamma-ray spectrometry of the Kimmeridge Clay, Dorset, UK. *Journal of the Geological Society, London*, **166**, 1123–1133.

van der Hoeven, I.C., Verreussel, R.M.C.H., Riboulleau, A., Tribovillard, N. and van de Schootbrugge, B. (2022) Climate-controlled organic matter accumulation as recorded in the Upper Jurassic Argiles de Châtillon Formation, a shallow-marine counterpart of the Kimmeridge Clay Formation. *Geological Magazine*, **160**: 579–600.

Hotinski, R.M. and Toggweiler, J.R. 2003. Impact of a Tethyan circumglobal passage on ocean heat transport and "equable" climates. *Paleoceanography*, **18**, 1–15.

Jach, R. and Rehákova, D. 2019. Middle to Late Jurassic carbonate-biosiliceous sedimentation and palaeoenvironment in the Tethyan Fatricum domain, Krížna Nappe, Tatra Mts, Western Carpathians. *Annales Societatis Geologorum Poloniae*, **89**, 1–46.

Jach, R., Rehákova, D. and Uchman, A. 2012. Biostratigraphy and palaeoenvironment of the Kimmeridgian–Lower Tithonian pelagic deposits of the Krížna Nappe, Lejowa Valley, Tatra Mts. (southern Poland). *Geological Quarterly*, **56**, 773–788.

Jach, R., Djerić, N., Goričan, Š. and Rehákova, D. 2014. Integrated stratigraphy of the Middle–Upper Jurassic of the Krížna Nappe, Tatra Mountains. *Annales Societatis Geologorum Poloniae*, **84**, 1–33.

Jackson, M. and Swanson-Hysell, N.L. 2012. Rock magnetism of remagnetized carbonate rocks: another look. *Geological Society, London, Special Publications*, **371**, 229–251.

Jenkyns, H.C. 1972. Pelagic "oolites" from the Tethyan Jurassic. *Journal of Geology*, **80**, 21–33.

Jenkyns, H.C. 1974. Origin of red nodular limestones (Ammonitico Rosso, Knollenkalke) in the Mediterranean Jurassic: a diagenetic model. *Special Publications of the International Association of Sedimentologists*, **1**, 249–271.

Jenkyns, H.C. 1999. Mesozoic anoxic events and palaeoclimate. *Zentralblatt für Geologie un Paläontologie, Teil I*, **7–9**, 943–949.

Jones, B. and Manning, A.C. 1994 Comparison of geochemical indices used for the interpretation of palaeoredox conditions in ancient mudstones. *Chemical Geology*, **111**, 111–129.

Jurewicz, E. 2005. Geodynamic evolution of the Tatra Mts. and the Pieniny Klippen Belt (Western Carpathians): problems and comments. *Acta Geologica Polonica*, **55**, 295–338.

Kotański, Z. 1959. Stratigraphical sections of the High-Tatric series in the Polish Tatra Mountains. *Biuletyn Instytutu Geologicznego*, **139**, 1–160. [In Polish with English summary]

Kotański, Z. 1961. Tectogenese et reconstitution de la paleogeographie de la zone Haut-Tatrique dans les Tatras. *Acta Geologica Polonica*, **11**, 187–476. [In Polish with French summary]

Kotański, Z. and Radwański, A. 1959. High-Tatric Tithonian in the Osobita region, its fauna with Pygope Diphya and products of volcanoes. *Acta Geologica Polonica*, **9**, 519–538. [In Polish with English summary]

Krobicki, M. 1994. Stratigraphic significance and palaeoecology of the Tithonian–Berriasian brachiopods in the Pieniny Klippen Belt, Carpathians, Poland. *Studia Geologica Polonica*, **106**, 89–156.

Kujau, A., Heimhofer, U., Hochuli, P.A., Pauly, S., Morales, C., Adatte, T., Föllmi, K., Ploch, I. and Mutterlose, J. 2013. Reconstructing Valanginian (Early Cretaceous) mid-latitude vegetation and climate dynamics based on spore-pollen assemblages. *Review of Palaeobotany and Palynology*, **197**, 50–69.

Lefeld, J. 1968. Stratigraphy and palaeogeography of the High-Tatric Lower Cretaceous in the Tatra Mountains. *Studia Geologica Polonica*, **24**, 1–115. [In Polish with English summary]

Lefeld, J. and Radwański, A. 1960. Les débris de Saccocoma dans les coupes du Malm et du Neocomien haut-tatrique des Tatras Polonaises. *Acta Geologica Polonica*, **10**, 593–618. [In Polish with French summary]

Lefeld, J., Gaździcki, A., Iwanow, A., Krajewski, K. and Wójcik, K. 1985. Jurassic and Cretaceous lithostratigraphic units of the Tatra Mountains. *Studia Geologica Polonica*, **84**, 7–93.

Leinfelder. R.R., Nose, M., Schmid, D.U. and Werner, W. 1993. Microbial crusts of the Late Jurassic: composition, palae-

oecological significance and importance in reef construction. *Facies*, **29**, 195–230.

Li, H.-Y. and Zhang, S.-H. 2005. Detection of mineralogical changes in pyrite using measurements of temperature-dependence susceptibilities. *Chinese Journal of Geophysics*, **48**, 1454–1461.

Li, Y.-H. and Schoonmaker, J.E. 2003. Chemical Compositions and Mineralogy of Marine Sediments. *Treatise on Geochemistry*, **7**, 1–35.

Liu, Q., Deng, C., Yu, Y., Torrent, J., Jackson, M.J., Banerjee, S.K. and Zhu, R. 2005. Temperature dependence of magnetic susceptibility in an argon environment: implications for pedogenesis of Chinese loess/palaeosols. *Geophysical Journal International*, **161**, 102–112.

Lodowski, D.G., Pszczółkowski, A., Szives, O., Főzy, I. and Grabowski, J. 2022a. Jurassic–Cretaceous transition in the Transdanubian Range (Hungary): integrated stratigraphy and paleomagnetic study of the Hárskút and Lókút sections. *Newsletters on Stratigraphy*, **55**, 99–135.

Lodowski, D.G., Pszczółkowski, A., Wilamowski, A. and Grabowski, J. 2022b. Jurassic–Cretaceous transition in the High-Tatric succession (Giewont Unit, Western Tatra Mts, Poland): integrated stratigraphy and microfacies. *Acta Geologica Polonica*, **72**, 107–135.

Lowrie, W. 1990. Identification of ferromagnetic minerals by coercivity and unblocking temperature properties. *Geophysical Research Letters*, **17**, 159–162.

Madzin, J., Sýkora, M. and Soták, J. 2014. Stratigraphic position of alkaline volcanic rocks in the autochtonous cover of the High-Tatric Unit (Western Tatra Mts., Central Western Carpathians, Slovakia). *Geological Quarterly*, **58**, 163–180.

McLennan, S.M. 2001. Weathering and global denudation. *The Journal of Geology*, **101**, 295–303.

Michalík, J. 2007. Sedimentary rock record and microfacies indicators of the latest Triassic to mid-Cretaceous tensional development of the Zliechov Basin (Central Western Carpathians). *Geologica Carpathica*, **58**, 443–453.

Michalík, J. and Vašíček, Z. 1987. Geology and stratigraphy of the Butkov Lower Cretaceous limestone deposits, Manín Unit, Middle Váh Valley (Western Slovakia). *Mineralia Slovaca*, **19**, 115–134. [In Slovak with English summary]

Michalík J., Reháková, D. and Vašíček, Z. 1995. Early Cretaceous sedimentary changes in West-Carpathian area. *Geologica Carpathica*, **46**, 285–296.

Michalík, J., Vašíček, Z., Skupien, P., Kratochvílova, L., Reháková, D. and Halásová, E. 2005. Lower Cretaceous sequences of the Manín Unit (Butkov Quarry, Strážovské vrchy Mts, Western Carpathians) – integrated biostratigraphy and sequence stratigraphy. *Slovak Geological Magazine*, **11**, 29–35.

Michalík, J., Lintnerová, O., Reháková, D., Boorová, D. and Šimo, V. 2012. Early Cretaceous sedimentary evolution of a pelagic basin margin (the Manín Unit, central Western Carpathians, Slovakia). *Cretaceous Research*, **38**, 68–79.

Michalík, J., Reháková, D., Grabowski, J., Lintnerová, O., Svobodová, A., Schlögl, J., Sobień, K. and Schnabl, P. 2016. Stratigraphy, plankton communities, and magnetic proxies at the Jurassic/Cretaceous boundary in the Pieniny Klippen Belt (Western Carpathians, Slovakia). *Geologica Carpathica*, **67**, 303–328.

Michalík, J, Bąk, M., Lintnerová, O. and Méres, Š. 2017. Biostratigraphy, geochemistry and sedimentology of Middle to Late Jurassic strata in the Strážovce section (Strážovské vrchy Mts), Krížna Nappe of the Central Carpathians, Slovakia. *Volumina Jurassica*, **XV**, 161–178.

Missoni, S. and Gawlick, H.-J. 2011. Jurassic mountain building and Mesozoic–Cenozoic geodynamic evolution of the Northern Calcareous Alps as proven in the Berchtesgaden Alps (Germany). *Facies*, **57**, 137–186.

Morales, C., Gardin, S., Schnyder, J., Spangenberg, J., Arnaud-Vanneau, A., Arnaud, H., Adatte, T. and Föllmi, K.B. 2013. Berriasian and early Valanginian environmental change along a transect from the Jura Platform to the Vocontian Basin. *Sedimentology*, **60**, 36–63.

Morgans-Bell, H.S., Coe, A.L., Hesselbo, S.P., Jenkyns, H.C., Weedon, G.P., Marshall, J.E.A., Tyson, E.V. and Williams, C.J. 2001. Integrated stratigraphy of the Kimmeridge Clay Formation (Upper Jurassic) based on exposures and boreholes in south Dorset, UK. *Geological Magazine*, **138**, 511–539.

Murphy, L.S. and Haugen, E.M. 1985. The distribution and abundance of phototrophic ultraplankton in the North Atlantic. *Limnology and Oceanography*, **30**, 47–58.

Muttoni, G., Erba, E., Kent, D.V. and Bachtadse, V. 2005. Mesozoic Alpine facies deposition as a result of past latitudinal plate motion. *Nature*, **434**, 59–63.

Nemčok, J., Bezák, V., Biely, A., Gorek, A., Gross, P., Halouzka, R., Janák, M., Kahan, Š., Kotański, Z., Lefeld, J., Mello, J., Reichwalder, P., Raczkowski, W., Roniewicz, P., Ryka, W., Wieczorek, J. and Zelman, J. 1994. Geological map of the Tatra Mountains. MŽP SR, GÚDŠ, Bratislava.

Nesbitt, H.W. and Young, G.M. 1982. Early Proterozoic climates and plate motions inferred from major element chemistry of lutites. *Nature*, **299**, 715–717.

Niebuhr, B. 2005. Geochemistry and time-series analyses of orbitally forced Upper Cretaceous marl-limestone rhytmites (Lehrte West Syncline, northern Germany). *Geological Magazine*, **142**, 31–55.

Ogg, J.G. 2020. Geomagnetic polarity time scale. In: Gradstein, F.M., Ogg, J.G., Schmitz, M.D. and Ogg, G.M. (Eds), The Geologic Time Scale 2020, 159–192. Elsevier; Amsterdam, London, Cambridge.

Oszczypko, N., Salata, D. and Krobicki, M. 2012. Early Cretaceous intra-plate volcanism in the Pieniny Klippen Belt – a case study of the Velykyi Kamenets'/Vilkhivchyk (Ukraine) and the Biała Woda (Poland) sections. *Geological Quarterly*, **56**, 629–648.

Plašienka, D. 1995. Passive and active margin history of the

northern Tatricum (Western Carpathians, Slovakia. *Geologische Rundschau*, **84**, 748–760.

Plašienka, D. 2003. Dynamics of Mesozoic pre-orogenic rifting in the Western Carpathians. *Mitteilungen der Österreichischen Geologischen Gesellschaft*, **94**, 79–98.

Plašienka, D. 2012. Jurassic syn-rift and Cretaceous syn-orogenic, coarse grained deposits related to opening and closure of the Vahic (South Penninic) Ocean in the Western Carpathians – an overview. *Geological Quarterly*, **56**, 601–628.

Plašienka, D. 2018. Continuity and episodicity in the early Alpine tectonic evolution of the Western Carpathians: How large-scale processes are expressed by the orogenic architecture and rock record data. *Tectonics*, **37**, 2029–2079.

Plašienka, D. 2019. Linkage of the Manín and Klape units with the Pieniny Klippen Belt and Central Western Carpathians: balancing the ambiguity. *Geologica Carpathica*, **70**, 35–61.

Plašienka, D. and Ožvoldová, L. 1996. New data about the age of radiolarites from the Belice Unit (Považský Inovec Mts., Central Western Carpathians). *Slovak Geological Magazine*, **1**, 21–26.

Pomar, L., Morsilli, M., Hallock, P. and Bádenas, B. 2012. Internal waves, an under-explored source of turbulence events in the sedimentary record. *Earth Science Reviews*, **111**, 56–81.

Price, G.D., Főzy, I. and Pálfy, J. 2016. Carbon cycle history through the Jurassic–Cretaceous boundary: A new global $\delta^{13}C$ stack. *Palaeogeography, Palaeoclimatology, Palaeoecology*. **451**, 46–61.

Pszczółkowski, A. 2018. Upper Jurassic bacteria from the Raptawicka Turnia Limestone Formation in the Mały Giewont area (Western Tatra Mountains, Poland), *Geological Quarterly*, **62**, 840–857.

Pszczółkowski, A., Grabowski, J. and Wilamowski, A. 2016. Integrated biostratigraphy and carbon isotope stratigraphy of the Upper Jurassic shallow water carbonates of the High-Tatric Unit (Mały Giewont area, Western Tatra Mountains, Poland). *Geological Quarterly*, **60**, 893–918.

Putiš, M., Soták, J., Li, Q.-L., Ondrejka, M., Li, X.-H., Hu, Z., Ling, X., Nemec, O., Németh, Z. and Ružička, P. 2019. Origin and age determination of the Neotethys Meliata Basin ophiolite fragments in the Late Jurassic–Early Cretaceous accretionary wedge mélange (Inner Western Carpathians, Slovakia). *Minerals*, **9**, 652.

Rais, P., Louis-Schmid, B., Bernasconi, M. and Weissert, H. 2007. Palaeogeographic and palaeoclimatic reorganization around the Middle–Late Jurassic transition. *Palaeogeography, Palaeoclimatology, Palaeoecology*, **251**, 527–546.

Rameil, N. 2005. Carbonate sedimentology, sequence stratigraphy, and cyclostratigraphy of the Tithonian in the Swiss and French Jura Mountains. A high-resolution record of changes in sea level and climate. Ph.D. thesis. *GeoFocus*, **13**, 246 pp.

Ray, D.C., van Buchem, F.S.P., Baines, G., Davies, A., Gréselle, B., Simmons, M.D. and Robson, C. 2019. The magnitude and cause of short-term eustatic Cretaceous sea-level change: A synthesis. *Earth-Science Reviews*, **197**, 102901.

Reháková, D. 2000. Calcareous dinoflagellate and calpionellid bioevents versus sea-level fluctuations recorded in the West-Carpathian (Late Jurassic/Early Cretaceous) pelagic environments. *Geologica Carpathica*, **51**, 229–243.

Riding, R. 1983. Cyanoliths (Cyanoids): Oncoids formed by calcified Cyanophytes. In: Peryt, T. (Ed.), Coated Grains, 276–283. Springer-Verlag; Berlin, Heidelberg.

Robbins, L.J., Lalonde, S.V., Planavsky, N.J., Partin, C.A., Reinhard, C.T., Kendall, B., Scott, C., Hardisty, D.S., Gill, B.C., Alessi, D.S., Dupont, C.L., Saito, M.A., Crowe, S.A., Poulton, S.W., Bekker, A., Lyons, T.W. and Konhauser, K.O. 2016. Trace elements at the intersection of marine biology and geochemical evolution. *Earth Science Reviews*, **163**, 323–348.

Rutsch, H.-J., Mangini, A., Bonani, G., Dittrich-Hannen, B., Kubik, P.W., Suter, M. and Segl, M. 1995. ^{10}Be and Ba concentrations in West African sediments trace productivity in the past. *Earth and Planetary Sciences Letters*, **133**, 129–143.

Satolli, S. and Turtù, A. 2016. Early Cretaceous magnetostratigraphy of the Salto del Cieco section (Northern Apennines, Italy). *Newsletters on Stratigraphy*, **49**, 361–382.

Schmid, S.M., Bernoulli, D., Fügenschuh, B., Matenco, L., Schefer, S., Schuster, R., Tischler, M. and Ustaszewski, K. 2008. The Alpine-Carpathian-Dinaridic orogenic system: correlation and evolution of tectonic units. *Swiss Journal of Geosciences*, **101**, 139–183.

Schneider, R.R. Price, B., Müller, P.J., Kroon. D. and Alexander, I. 1997. Monsoon related variations in Zaire (Congo) sediment load and influence of fluvial silicate supply on marine productivity in the east equatorial Atlantic during the last 200,000 years. *Paleoceanography*, **12**, 463–481.

Schnetger, B., Brumsack, H.-J., Schale, H., Hinrichs, J. and Dittert, L. 2000. Geochemical characteristics of deep-sea sediments from the Arabian Sea: a high-resolution study. *Deep-Sea Research II*, **47**, 2735–2768.

Shen, J., Schoepfer, S.D., Feng, Q., Zhou, L., Yu, J., Song, H., Wei, H. and Algeo, T.J. 2015. Marine productivity changes during the end-Permian crisis and Early Triassic recovery. *Earth-Science Reviews*, **149**, 136–162.

Sidhu, P.S., Gilkes, R.J. and Posner, A.M. 1977. Mechanism of the low temperature oxidation of synthetic magnetites. *Journal of Inorganic and Nuclear Chemistry*, **39**, 1953–1958.

Soták, J., Plašienka, D., Spišiak, J. and Uher, P. 1993. Neptunian carbonate dykes hosted by basic volcanic rocks in the Považský Inovec Mts. (Western Carpathians). *Mineralia Slovaka*, **25**, 193–201. [In Slovak with English summary]

Stampfli, G.M. and Hochard, C. 2009. Plate tectonics of the Alpine realm. In: Murphy, J.B., Keppie, J.D., Hynes, A.J. (Eds), Ancient Orogens and Modern Analogues. *Geological Society, London, Special Publications*, **327**, 89–111.

Staniszewska, A. and Ciborowski, T. 2000. Lower Cretaceous breccia from autochthonous High-Tatric succession in Western Tatra Mts. *Przegląd Geologiczny*, **48**, 246–250. [In Polish with English summary]

Steiner, T.M.C., Gawlick, H.-J., Melcher, F. and Schlagintweit, F. 2021. Ophiolite derived material as parent rocks for Late Jurassic bauxite: evidence for Tithonian unroofing in the Northern Calcareous Alps (Eastern Alps, Austria). *International Journal of Earth Sciences*, **110**, 1847–1862.

Sutton, T.T. 2013. Vertical ecology of the pelagic ocean: classical patterns and new perspectives. *Journal of Fish Biology*, **83**, 1508–1527.

Szederkényi, T., Haas, J., Nagymarosy, A. and Hámor, G. 2013. Geology and History of Evolution of the Tisza Mega-Unit. In: Haas, J. (Ed.), *Geology of Hungary*, 244 pp. Springer; Heidelberg, New York, Dordrecht, London.

Tian, J., Xie, X., Ma, W., Jin, H. and Wang, P. 2011. X-ray fluorescence core scanning records of chemical weathering and monsoon evolution over the past 5 Myr in the southern South China Sea. *Paleoceanography*, **26**, PA4202.

Tribovillard, N., Algeo, T.J., Lyons, T. and Riboulleau, A. 2006. Trace metals as paleoredox and paleoproductivity proxies: An update. *Chemical Geology*, **232**, 12–32.

Turner, H.E. 2018. Integrated correlation of the Kimmeridge Clay Formation (Late Jurassic–Early Cretaceous): a Boreal–Tethyan transect, 212 pp. Ph.D. Thesis, University of Portsmouth, Portsmouth, UK. https://researchportal.port.ac.uk/en/studentTheses/integrated-correlation-of-the-kimmeridge-clay-formation-late-jura

Turner, H.E. and Huggett, J.M. 2019. Late Jurassic–Early Cretaceous climate change record in clay minerals of the Norwegian-Greenland Seaway. *Palaeogeography, Palaeoclimatology, Palaeoecology*, **534**, 109331.

van Velzen, A. 1992. Magnetic minerals in Pliocene and Pleistocene marine marls from Southern Italy. Rock magnetic properties and alteration during thermal demagnetization. *Geologica Ultraiectina*, **122**, 154 pp.

Védrine, S., Strasser, A. and Hug, W. 2007. Oncoid growth and distribution controlled by sea-level fluctuations and climate (Late Oxfordian, Swiss Jura Mountains). *Facies*, **53**, 535–552.

Walker, T.R. 1984. Diagenetic albitization of potassium feldspar in arkosic sandstones. *SEPM Journal of Sedimentary Research*, **54**, 3–16.

Waters, K.E., Rowson, N.A., Greenwood, R.W. and Williams, A.J. 2008. The effect of heat treatment on the magnetic properties of pyrite. *Minerals Engineering*, **21**, 679–682.

Wei, G., Liu, Y., Li, X., Shao, L. and Liang, X. 2003. Climatic impact on Al, K, Sc and Ti in marine sediments: Evidence from ODP Site 1144, South China Sea. *Geochemical Journal*, **37**, 593–602.

Wei, G., Li, X.-H., Liu, Y., Shao, L. and Liang, X. 2006. Geochemical record of chemical weathering and monsoon climate change since the early Miocene in the South China. *Paleoceanography*, **21**, PA4214.

van der Weijden, C.H., Reichart, G.-J. and van Os, B.J.H. 2006. Sedimentary trace elements records over the last 200 kyr from within and below the northern Arabian Sea oxygen minimum zone. *Marine Geology*, **231**, 69–88.

Weissert, H. and Channell., J.E.T. 1989. Tethyan carbonate carbon isotope stratigraphy across the Jurassic–Cretaceous boundary: an indicator of decelerated global carbon cycling? *Paleoceanography*, **4**, 483–494.

Weissert, H. and Mohr, H. 1996. Late Jurassic climate and its impact on carbon cycling. *Palaeogeography, Palaeoclimatology, Palaeoecology*, **122**, 27–43.

Weissert, H. and Erba, E. 2004. Volcanism, CO_2 and palaeoclimate: a Late Jurassic–Early Cretaceous carbon and oxygen isotope record. *Journal of the Geological Society, London*, **161**, 695–702.

Weissert, H., Lini, A., Föllmi, K.B. and Kuhn, O. 1998. Correlation of Early Cretaceous carbon isotope stratigraphy and platform drowning events: a possible link? *Palaeogeography, Palaeoclimatology, Palaeoecology*, **137**, 189–203.

Westermann, S., Duchamp-Alphonse, S., Fiet, N., Fleitmann, V., Adatte, T. and Föllmi, K.B. 2013. Palaeoenvironmental changes during the Valanginian: New insights from variations in phosphorus contents and bulk- and clay mineralogies in the western Tethys. *Palaeogeography, Palaeoclimatology, Palaeoecology*, **392**, 196–208.

Wierzbowski, H., Anczkiewicz, R., Pawlak, J., Rogov, M.A. and Kuznetsov, A.B. 2017. Revised Middle–Upper Jurassic strontium isotope stratigraphy. *Chemical Geology*, **446**, 239–255.

Manuscript submitted: 4th November 2022
Revised version accepted: 21st August 2023